TECHNICAL REPORT R-46

PRESSURE AND FORCE CHARACTERISTICS OF NONCIRCULAR CYLINDERS AS AFFECTED BY REYNOLDS NUMBER WITH A METHOD INCLUDED FOR DETERMINING THE POTENTIAL FLOW ABOUT ARBITRARY SHAPES

By EDWARD C. POLHAMUS, EDWARD W. GELLER,
and KALMAN J. GRUNWALD

Langley Research Center
Langley Field, Va.

TECHNICAL REPORT R-46

PRESSURE AND FORCE CHARACTERISTICS OF NONCIRCULAR CYLINDERS AS AFFECTED BY REYNOLDS NUMBER WITH A METHOD INCLUDED FOR DETERMINING THE POTENTIAL FLOW ABOUT ARBITRARY SHAPES

By Edward C. Polhamus, Edward W. Geller, and Kalman J. Grunwald

SUMMARY

The low-speed pressure distribution and force characteristics of several noncircular two-dimensional cylinders have been measured in a wind tunnel through a range of Reynolds numbers and flow incidences. The flow incidences are analogous to the angle of attack of a two-dimensional airfoil and in addition correspond to combined angles of attack and sideslip in the crossflow plane of three-dimensional bodies. In view of this correspondence the force results are discussed in terms of the directional stability and spinning characteristics of fuselages at high angles of attack. Large effects of Reynolds number were encountered in both the overall forces and the distribution of the pressures. A method of determining the potential-flow pressure distribution for arbitrary cross sections is developed and the results are compared with experiment.

INTRODUCTION

Wind-tunnel studies (ref. 1) of the aerodynamic characteristics of various two-dimensional noncircular cylinders with axes normal to the stream have indicated large effects of cross-sectional shape, Reynolds number, and flow incidence (analogous to angle of attack of two-dimensional airfoils and obtained by rotating the cylinders about their axes). The side force was found to be especially critical and very often underwent a change in sign with a change in Reynolds number. Inasmuch as the flow incidence is analogous to that in the cross-flow plane of fuselages at combined angles of attack and sideslip, reference 1 presented a method of applying the two-dimensional results to the prediction of the sideslip and spin characteristics of fuselages at high angles of attack. Correlations with fuselage results indicated that the effect of cross section could be predicted and that the effect of Reynolds number was especially important in the case of flat spins. In order to determine the flow phenomena associated with the rather large Reynolds number effects and to provide information with which estimates of fuselage load distributions might be made, it appeared desirable to obtain the pressure distribution around the various cylinders.

The purpose of the present investigation, therefore, is to determine the pressure distributions associated with the large changes in the aerodynamic characteristics which accompany changes in Reynolds number. Also, since a reasonable correlation with the sideslip and spin characteristics of fuselages was obtained in reference 1, the investigation was extended to cover additional cross-sectional shapes which might be of interest. In order to allow correlations with experiment and theory, the potential-flow pressure distributions were calculated for cross sections similar to those tested. In addition, theoretical solutions for several systematic series of cross sections were determined, since a knowledge of the potential-flow pressure distributions was believed to be useful in predicting the type of flow that might be encountered in the real fluid for various cross sections.

SYMBOLS

The convention used with regard to flow inclination, cylinder reference dimensions, and the direction and positive sense of the aerodynamic coefficients are presented in figure 1. The aerodynamic coefficients and Reynolds numbers have been corrected for the effects of the wind-tunnel walls by the method of reference 2. Forces are presented relative to the body axes, and the symbols used are defined as follows:

a, l, β — variable geometric quantities used in transforming a circle to an arbitrary shape

b — maximum projected width of cylinder normal to flow for given flow incidence (see fig. 1)

b_o — maximum width of cylinder normal to flow at zero flow incidence (see fig. 1)

c_d — section drag coefficient, $\frac{\text{Force in stream direction per unit length}}{b\frac{\rho}{2}V_\infty^2}$

c_o — maximum depth of cylinder parallel to flow at zero flow incidence (see fig. 1)

C_p — pressure coefficient, $\frac{\text{Local static pressure}-\text{Free-stream static pressure}}{\frac{\rho}{2}V_\infty^2}$

$C_{p,z}$ — pressure coefficient in complex z-plane

$C_{p,\zeta}$ — pressure coefficient in complex ζ-plane

c_x — section longitudinal-force coefficient, $\frac{\text{Longitudinal force per unit length}}{b_o\frac{\rho}{2}V^2}$

c_y — section side-force coefficient, $\frac{\text{Side force per unit length}}{b_o\frac{\rho}{2}V_\infty^2}$

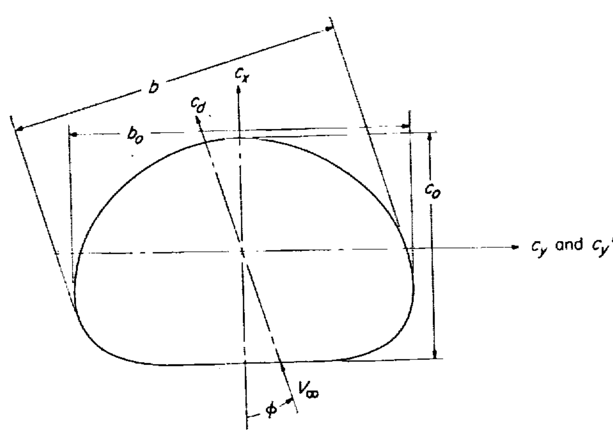

FIGURE 1. Convention used to define positive sense of flow inclination, cylinder reference dimensions, and aerodynamic coefficients.

c_y' — section side-force coefficient based on c_o instead of b_o

M — Mach number

N_{Re} — Reynolds number, based on c_o (except where noted otherwise)

r — corner radius of cylinder

R — radius of circle used in conformal transformation

V_s — sinking speed of aircraft

V_z — complex velocity in z-plane

V_ζ — complex velocity in ζ-plane

V_∞ — free-stream velocity (see fig. 1)

x,y — variables in complex z-plane

z — complex variable $(x+iy)$

ρ — free-stream air density

ϕ — flow incidence in plane normal to axis of cylinder (see fig. 1)

ξ,η — variables in complex ζ-plane

ζ — complex variable $(\xi+i\eta)$

MODELS

Sketches of the various cross sections of the cylinders tested are presented in figure 2, and a photograph of the cylinder having a modified triangular cross section mounted in the wind tunnel is shown in figure 3. The models were constructed of mahogany and were lacquered to produce smooth surfaces. Figures 4 to 6 present comparisons of the contours of the experimental cylinders with those for which theoretical solutions for the pressure distributions were either available or developed in the appendix. It should be pointed out that the experimental force data for most of the cylinders shown in figures 4 to 6 are presented in reference 1 and only a selected part of these data are included in the present report to provide a correlation with the experimental and theoretical pressure distributions. In figure 7 comparison is made of the contours of two of the experimental cylinders which have similar third and fourth quadrants. The orifice locations at which the experimental pressures were measured are indicated in figure 8.

TESTS

The cylinders were tested in the Langley 300-MPH 7- by 10-foot tunnel and spanned the tunnel from floor to ceiling as shown in figure 3. Figure 3 also shows the end plates, which were used to minimize any effects that might be caused by air leakage through the small clearance gaps

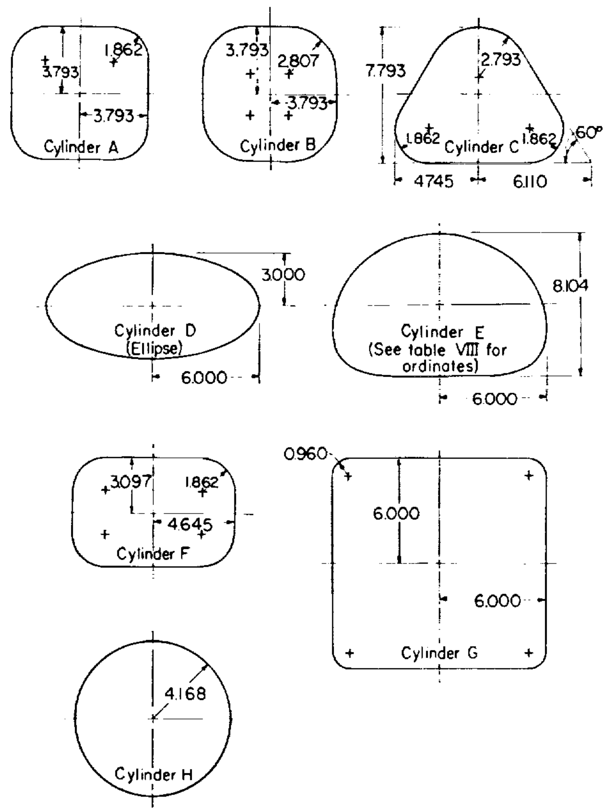

Source of Basic Data

Cylinder	A	B	C	D	E	F	G	H
Force measurements.	Ref. 1	Herein	Ref. 1 and herein	Herein	Herein	Ref. 1	Ref. 1	Ref. 1
Pressure measurements.	Herein	--------	Herein	--------	--------	--------	--------	--------

FIGURE 2.—Cross-sectional details of two-dimensional cylinders tested at various flow incidences in the Langley 300-MPH 7- by 10-foot tunnel.

required for the cylinders to pass through the floor and ceiling. In an attempt to determine whether any appreciable interference remained and to verify the low turbulence level of the tunnel, a circular cylinder was tested and the results are compared in reference 1 with results obtained by other investigators. These results indicated that no serious interference effects existed, and it is assumed that this is also true for the noncircular cylinders.

The forces developed by the various cylinders were measured by the standard mechanical balance system of the tunnel, and the pressure distributions (tables I to III) were obtained by means of orifices (fig. 8) in the cylinder surface with pressure leads to an alcohol manometer board.

Inasmuch as the Reynolds number variation was obtained by velocity variation rather than density or scale variation, a change in Reynolds number is accompanied by a variation in Mach number. In order to determine to what extent this might affect the experimental results, the theoretical critical Mach numbers (free-stream Mach number for which speed of sound is first reached on body) have been estimated for several

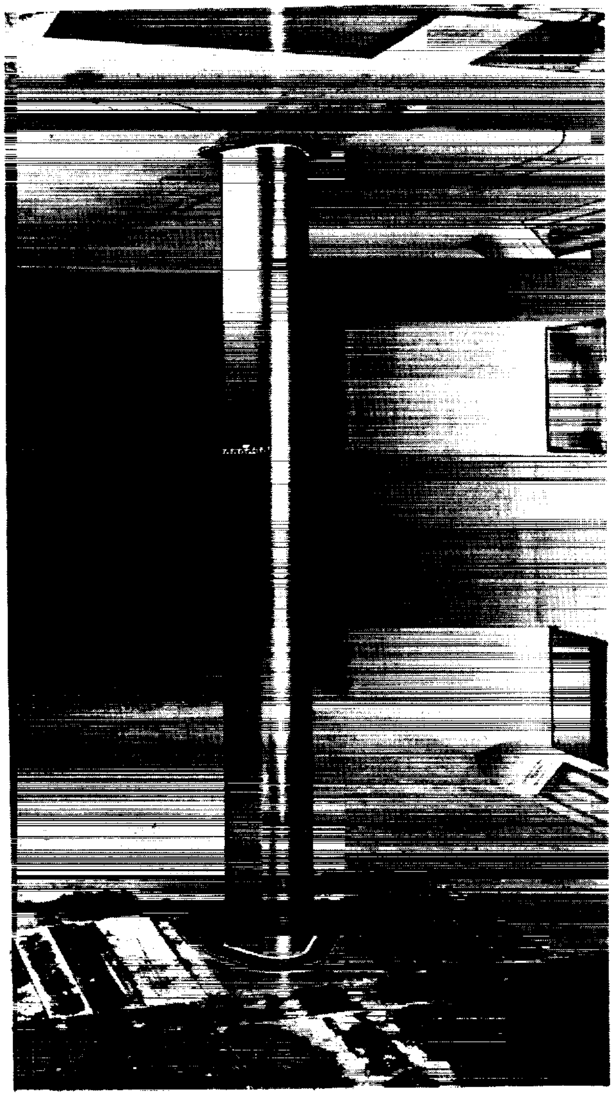

FIGURE 3.—Photograph of modified triangular cylinder mounted in tunnel (taken from downstream).

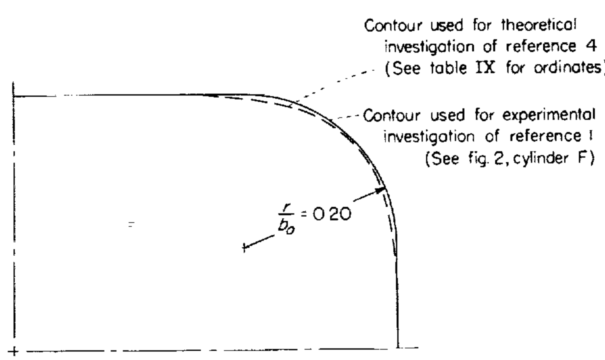

FIGURE 4.—Contour details of one quadrant of modified rectangular cross sections used for theoretical and experimental investigations.

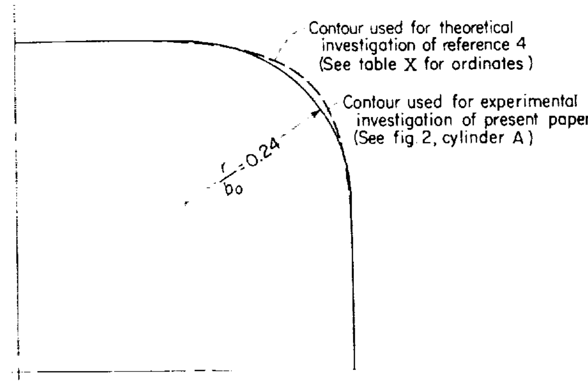

FIGURE 5.—Contour details of one quadrant of modified square cross sections used for theoretical and experimental investigations.

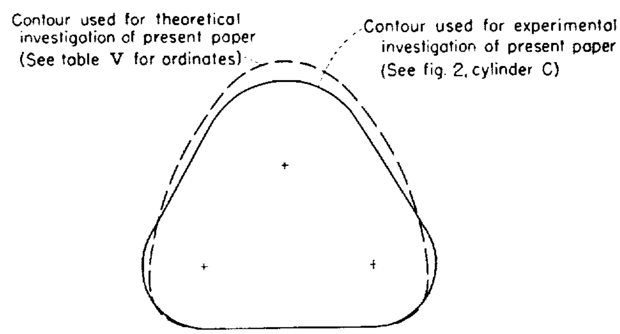

FIGURE 6.—Contour details of modified triangular cross sections used for theoretical and experimental investigations.

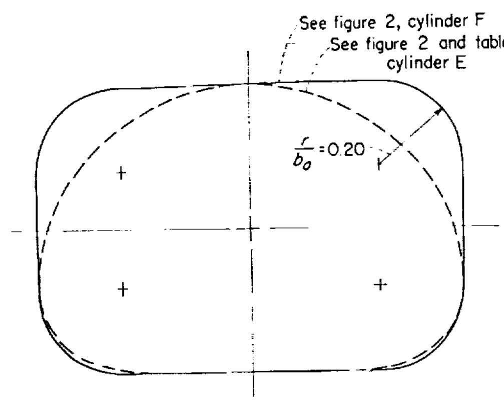

FIGURE 7.—Contour details of two experimental cylinders having similar third and fourth quadrants.

series of cross sections and the results are presented in figure 9. The critical Mach numbers were estimated with the aid of the theoretical incompressible minimum pressure coefficient (see tables IV to XI) and of the Prandtl-Glauert rule. The

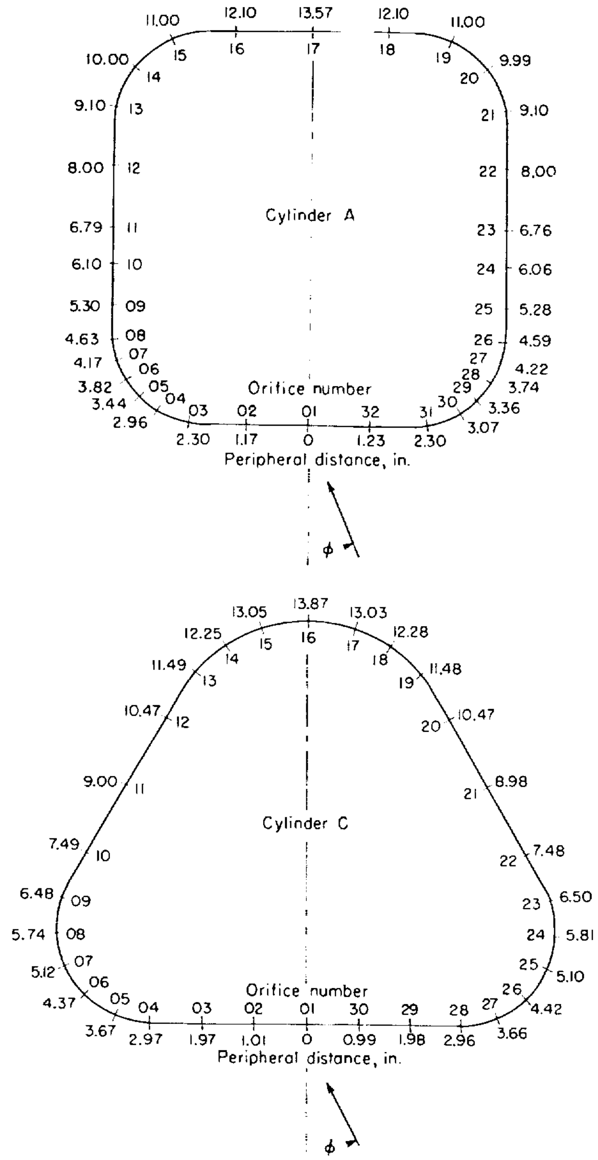

FIGURE 8.—Orifice locations in modified square and triangular cylinders.

critical Mach numbers are shown for both zero incidence and 30° incidence. The 30° incidence was selected because, for most of the cross sections, it produced the minimum pressure for the flow angles used. Also shown in figure 9 is the test Mach number range (hatched bars), and except for a small region for the flat ellipse and the triangle, the critical Mach number was apparently not reached. It appears reasonable, therefore, to assume that, at least with regard to large variations in aerodynamic characteristics, the effect of Reynolds number is predominant.

THEORY

For the purpose of providing information that would assist in analyzing the measured Reynolds number effects and in anticipating the type of Reynolds number effects that might be encountered with other cross sections, pressure distributions were determined from potential theory (with no circulation). It is believed that the knowledge that can be gained by comparing theory and experiment (such as the relationship between theoretical pressure gradients, flow separation, and Reynolds numbers) might be sufficient to allow the general characteristics of other shapes to be predicted to some extent. For example, with this knowledge and the theoretical pressure distribution, the order of occurrence of separation at the various corners might be predicted and thereby an indication might be provided of at least the direction of the side force that might be developed in various Reynolds number ranges. The purpose of this section therefore is to mention briefly the theoretical methods used to determine the potential-flow pressure distribution about the various cross sections.

The potential-flow pressure distributions about various cross sections can be obtained by the transformation of the flow about a circle by the use of complex variables, and the general procedure is described in many text books. The specific application of the method required to determine the potential-flow pressure distribution about the elliptical cross sections is also readily available in various texts (ref. 3, for example) and therefore is not included herein. In reference 4, Maruhn applied the general transformation to the specific cases of various rectangular cross sections having several degrees of corner rounding. In addition to the surface velocities and pressures, Maruhn presents the field velocities which are useful in determining the rolling moments due to sideslip for various wing-body combinations. In the present paper the method of reference 4 is used to determine the pressure distribution about the rectangular cross sections.

Application of the method to the determination of the pressures about various modified triangular cross sections is described in appendix A and a general method useful for arbitrary cross sections is developed in appendix B.

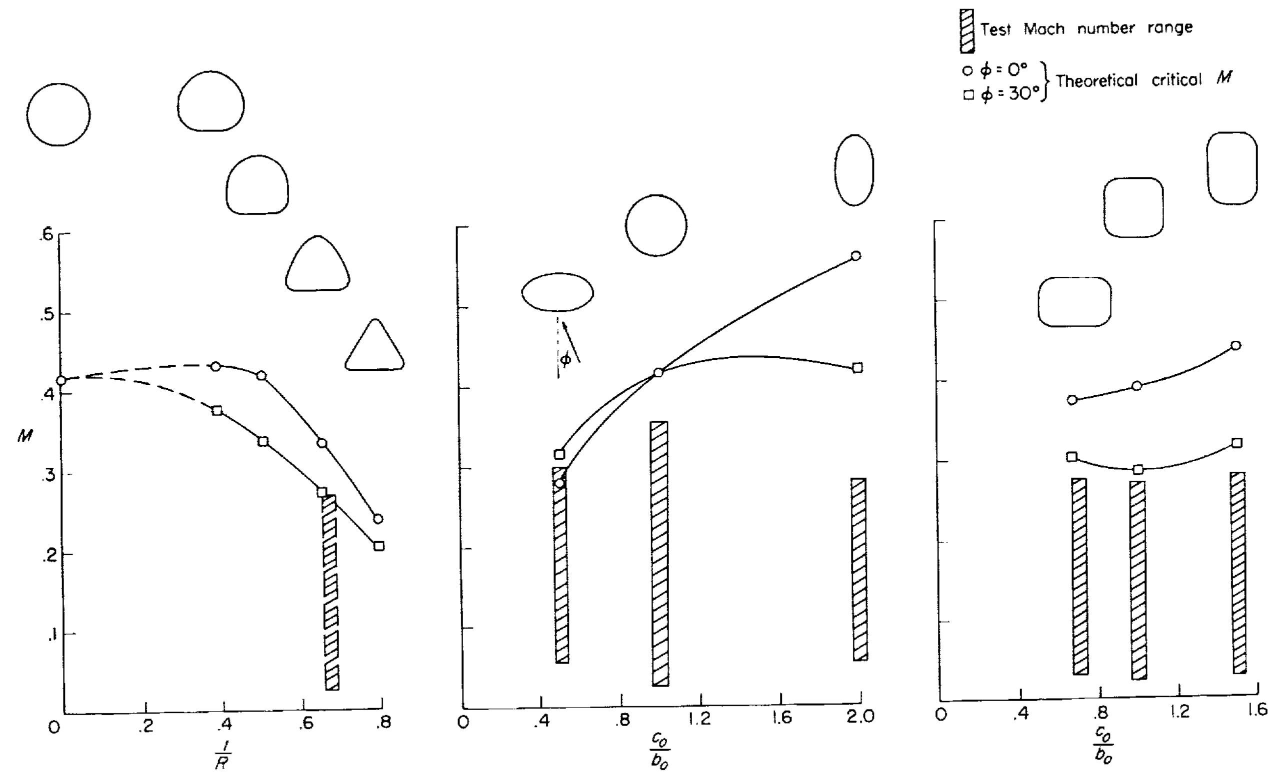

FIGURE 9.—Comparison of theoretical critical Mach numbers and test Mach number ranges.

RESULTS AND DISCUSSION

Presented in figures 10 to 14 are the basic force coefficients c_x and c_y as a function of Reynolds number (based on c_o) for various flow incidences. Care must be exercised in using these data to remember that measurements were taken relative to the body rather than the wind axes and that for the basic data both coefficients are based on b_o, the maximum width of the cylinder normal to the stream at $\phi=0°$. (See fig. 1.) A common reference length is, of course, desirable when both force components are presented; however, in the summary figures where side force alone is presented the coefficient is based on c_o (see fig. 1) and indicated by a prime. Although the results, of course, could just as well have been presented in terms of lift coefficients and angles of attack, the present system was selected because it was expected that the major application might be in connection with the side force developed on noncircular fuselages in flat spins or during sideslip excursions at high angles of attack.

The experimental pressure-distribution results are presented in tables I to III and the theoretical pressure-distribution results in tables IV to XI.

FORCE CHARACTERISTICS

At this point a few general comments are made with regard to the force characteristics; more detailed comments are made subsequently in connection with the discussion of the pressure distributions. Inasmuch as the drag characteristics of a large number of cross sections have been presented in references 1 and 5, the discussion here will, for the most part, be limited to the side-force characteristics. There is, however, an interesting point with regard to the drag of the square cylinder having the corner radius of $0.37b_o$ shown in figure 10(a). The results indicate that the subcritical drag coefficient of this square cylinder is approximately 42 percent lower than that developed by a circular cylinder and that the effect of Reynolds number is rather small. This low subcritical drag coefficient may be explained by the rather large constant pressure section and the reduction in the maximum negative pressure relative to the circle that would be expected (by interpolating between the pressure coefficients of table X and those for a circle) for the square with

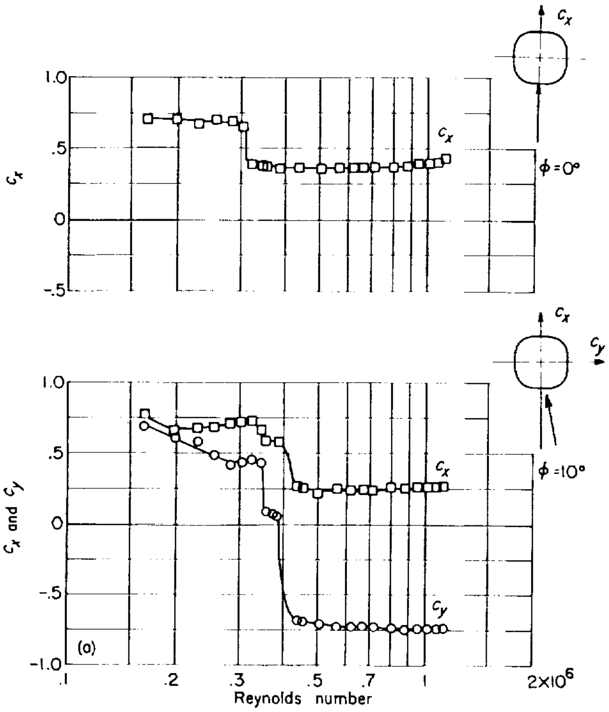

(a) $\phi=0°$ and 10°

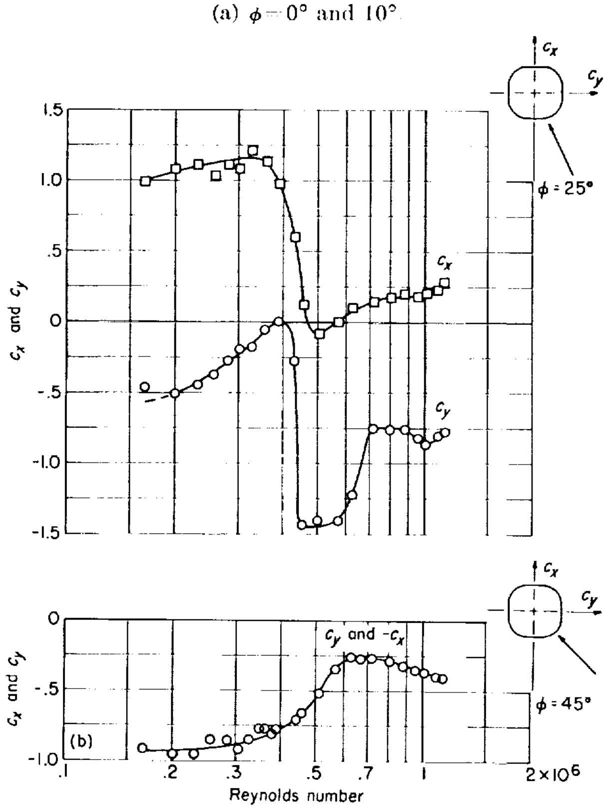

(b) $\phi=25°$ and 45°.

FIGURE 10. Effect of Reynolds number and flow incidence on force characteristics of a square cylinder. $r/b_o=0.370$.

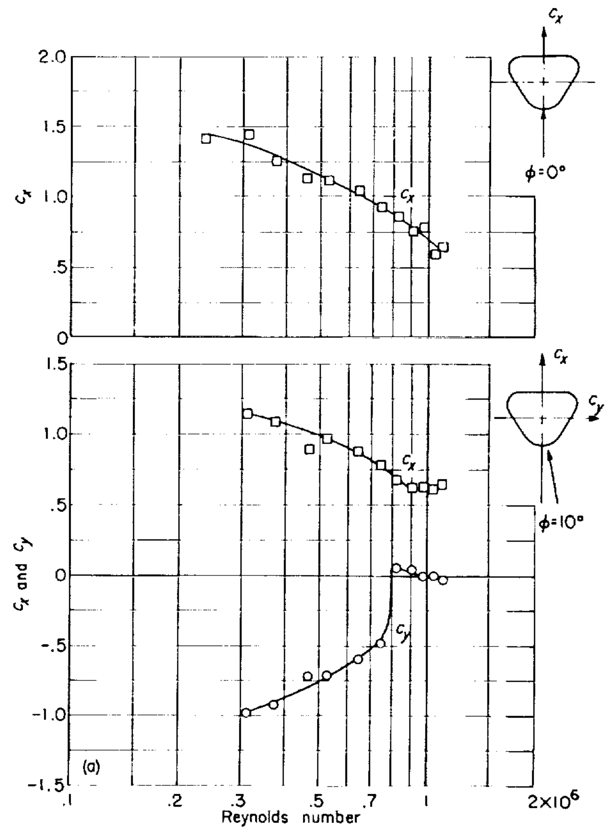

(a) $\phi=0°$ and 10°.

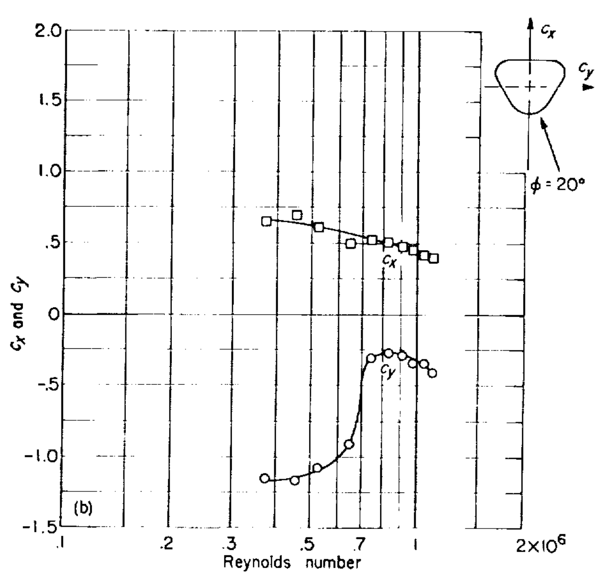

(b) $\phi=20°$.

FIGURE 11.—Effect of Reynolds number and flow incidence on the force characteristics of an inverted triangular cylinder. (Coefficients based on b_o.)

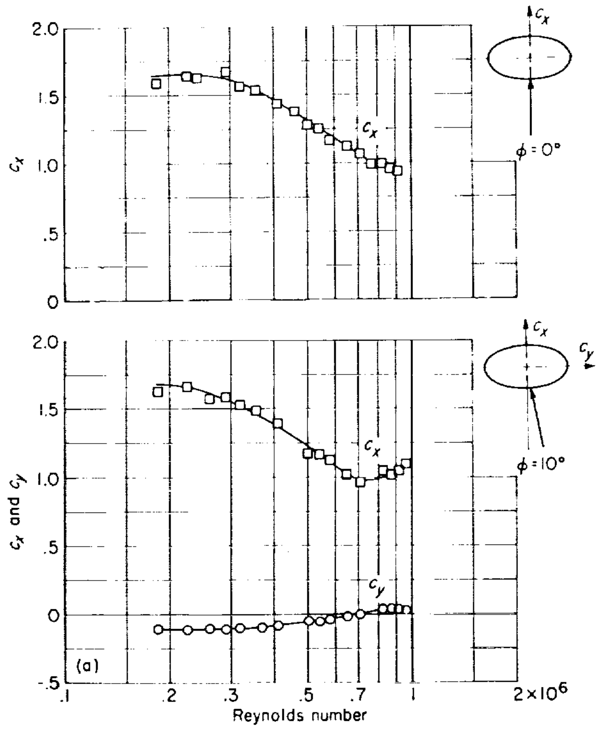

(a) $\phi = 0°$ and $10°$.

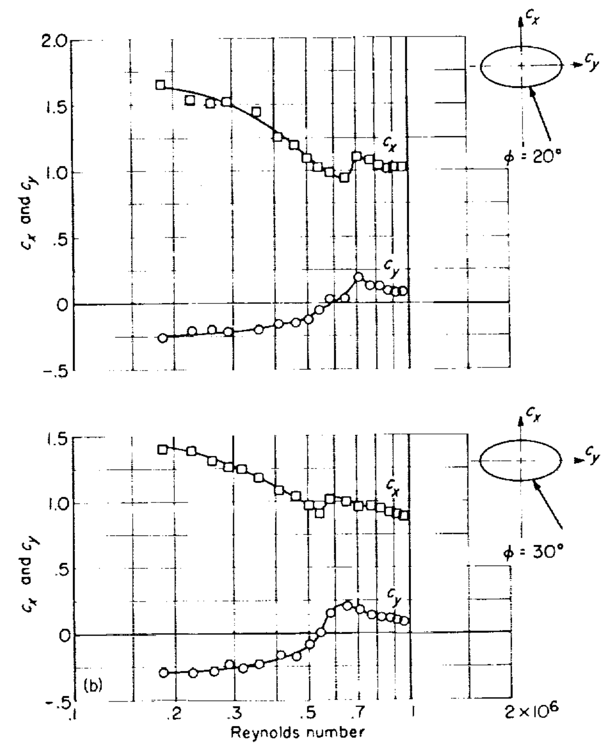

(b) $\phi = 20°$ and $30°$.

FIGURE 12.—Effect of Reynolds number and flow incidence on the force characteristics of an elliptic cylinder. $c_o/b_o = 0.5$. (Coefficients based on b_o.)

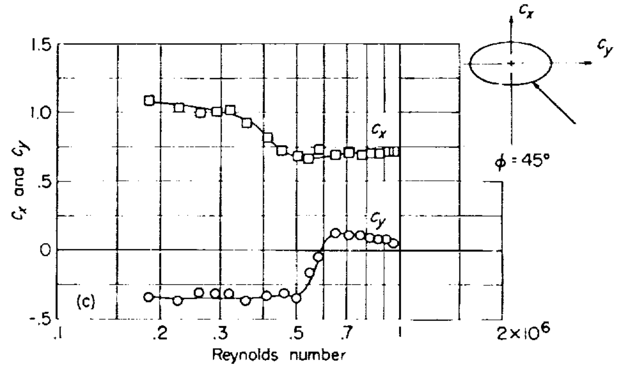

(c) $\phi = 45°$.

FIGURE 12.—Concluded.

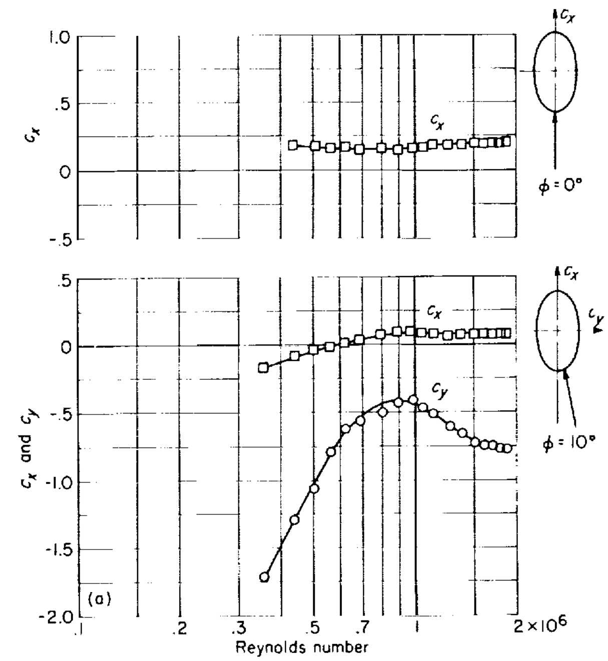

(a) $\phi = 0°$ and $10°$.

FIGURE 13.—Effect of Reynolds number and flow incidence on the force characteristics of an elliptic cylinder. $c_o/b_o = 2.0$. (Coefficients based on b_o.)

corner radii of $0.37b_o$. Further investigation of the effect of radius would appear desirable, since a cross section closely resembling a circle but having low drag at subcritical Reynolds numbers might be of value in connection with low-scale wind-tunnel stability and spin investigations, provided that little side force was developed.

The side-force results obtained for the square cylinder having a radius of $0.37b_o$ (see fig. 10) are quite similar, with regard to Reynolds number effects, to those obtained with a radius of $0.24b_o$. (See ref. 1.) Of particular interest is the result

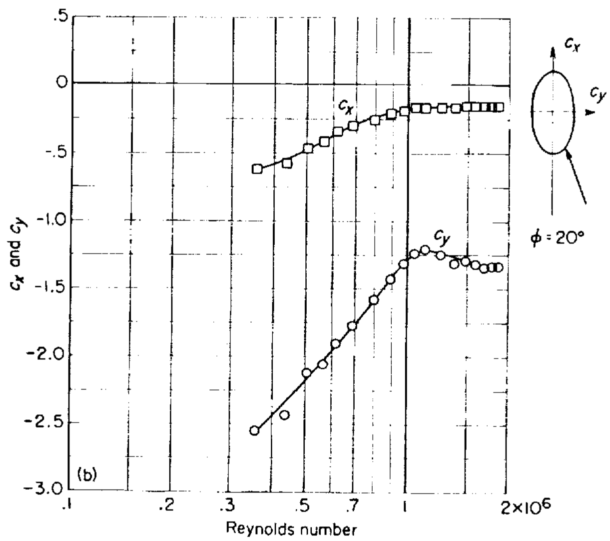

(b) $\phi=20°$.

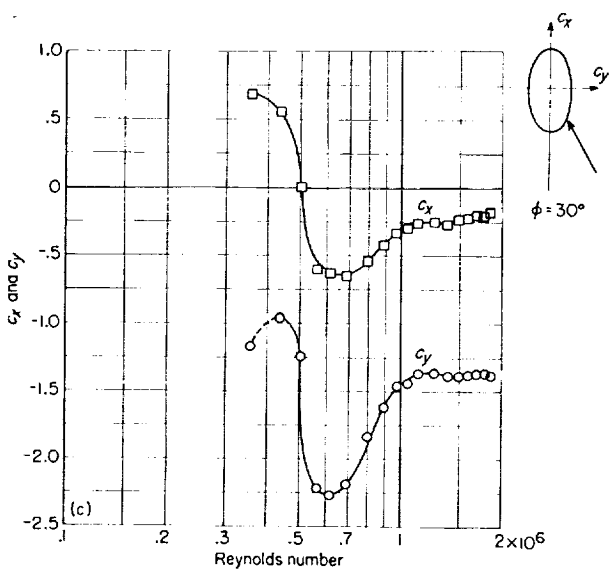

(c) $\phi=30°$.

FIGURE 13.—Concluded.

that rather large values of side force are developed despite the fact that the cross section is considerably closer to a circle than that of reference 1. The relationship between corner radius and side force for a flow incidence of 10° can better be seen in figure 15. In this figure the side-force coefficient c_y' is presented as a function of Reynolds number for various corner radii. As might be expected the critical Reynolds number decreases with increasing corner radius. At supercritical Reynolds numbers the side force developed by the square having the corner radii of $0.24b_o$ approaches

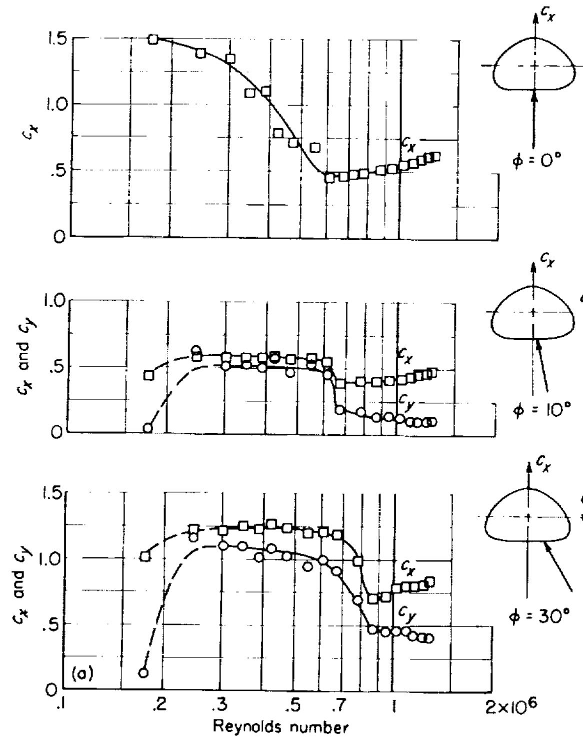

(a) $\phi=0°$, 10°, and 30°.

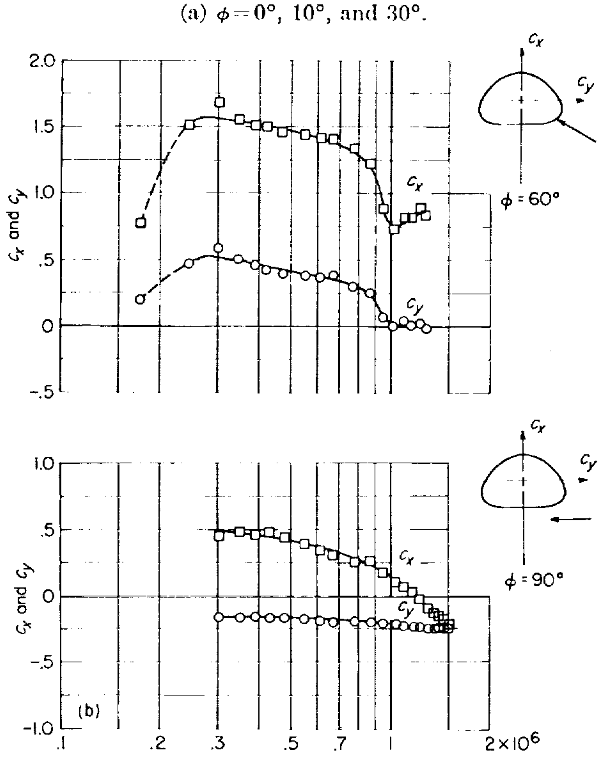

(b) $\phi=60°$ and 90°.

FIGURE 14.—Effect of Reynolds number and flow incidence on the force characteristics of a flat-front cylinder. (Coefficients based on b_o.)

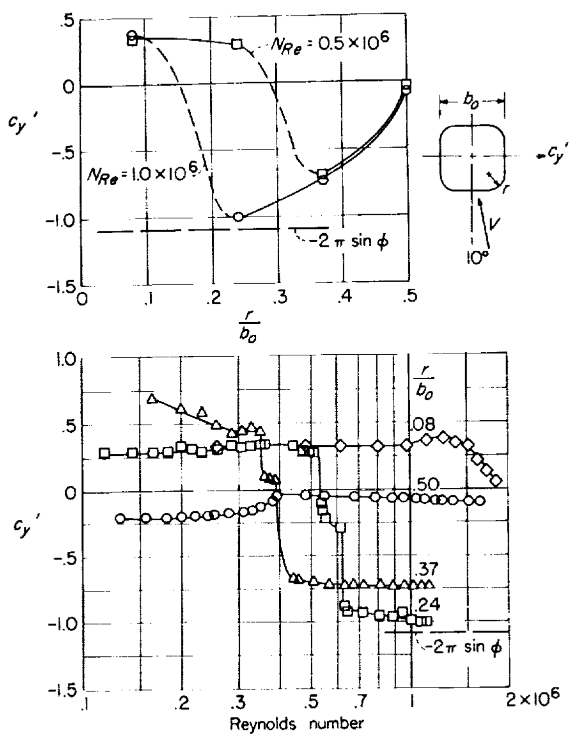

FIGURE 15. Effect of corner radius on c_y' at $\phi=10°$.

that predicted for a flat plate ($-2\pi \sin \phi$), while that developed by the square having the corner radii of $0.37b_o$ is approximately 62 percent of the flat-plate value. Because of the relatively high value of the critical Reynolds number for the square having the corner radii of $0.08b_o$ the complete transition was not obtained for this case and therefore the supercritical value of side force was not determined. Also shown in figure 15 is the side-force variation for a corner radius of $0.50b_o$, which, of course, corresponds to a circular cylinder. This variation was determined by multiplying the drag of a circular cylinder (ref. 1) by ($-\sin \phi$) in order to determine the component in the side-force direction. Also shown in figure 15 is the variation of c_y' with r/b_o for $\phi=10°$ at $N_{Re}=1.0\times10^6$ and 0.5×10^6.

Regarding the inverted triangular cross section (fig. 11), the results indicate large negative side forces being developed at the lower Reynolds numbers. These side forces diminish rather rapidly with increasing Reynolds number, presumably because of the relatively large trailing-edge corner radii. It is of interest to note that the low Reynolds number results are in qualitative agreement with those obtained for a sharp-corner inverted triangular cross section at a Reynolds number of about 0.20×10^6 in reference 6 when converted to the present axis and sign conventions. Data for higher Reynolds number were not obtained for the sharp-corner triangle, but it might be expected that the large side forces would be maintained to rather high Reynolds number as a result of the extreme pressure gradients that would be involved in any flow attachment around the corners.

The results obtained for two elliptic cylinders are presented in figures 12 and 13 for c_o/b_o ratios of 0.5 and 2.0, respectively. These results indicate that the cylinder having a c_o/b_o ratio of 2.0 developed by far the greatest side forces. This result would be expected, of course; however, the extremely large Reynolds number effects are of interest. Similar effects have been observed by other investigators for various values of c_o/b_o (refs. 7 and 8), and these effects are discussed further in connection with the pressure distribution in a subsequent section. It might be mentioned, however, that a considerable amount of leading-edge suction is indicated (see fig. 13(b), for example) for this cylinder and that it also is considerably dependent upon Reynolds number.

The side-force characteristics obtained with the flat triangular cross section (fig. 14) are considerably different from those obtained with the flat ellipse and experience a rather sharp transition similar to the flat rectangle (ref. 1). However, the change in sign of the side force experienced by the rectangle at supercritical Reynolds numbers is not experienced by the flat triangle. Of interest in connection with the autorotative characteristics of this type of cross section is Lanchester's discussion of the "aerial tourbillion." (See page 30 of ref. 9.)

PRESSURE DISTRIBUTIONS

In order to afford a better understanding of the side-force characteristics of various two-dimensional cylinders presented in the previous section and in reference 1, an experimental and theoretical study of the pressure distributions around several of the cross sections was undertaken. It was also believed that the results obtained might provide an indication of the type of fuselage load distributions that might be encountered during sideslip excursions at high angles of attack or during flat spins. It should be kept in mind that the theoretical calculations are for zero circulation except for the airfoil section where the sharp trailing edge assures Kutta type of flow.

The theoretical pressure distributions were determined by the methods described in the section on "Theory" and are presented in tables IV to XI. In addition to solutions for the cross sections which approach or are identical to those used in the experimental phase, solutions for several other cross sections were obtained, since it was believed that a knowledge of the potential-flow pressure distribution might be of aid in predicting the type of Reynolds number effects that may be encountered.

The experimentally determined pressure coefficients are presented in tables I to III and these pressures for a few conditions are presented in vector form in figures 16 to 18, along with the theoretical distribution and the corresponding force data.

Square cylinder. Some results obtained for the square cylinder having corner radii of $0.24b_o$ are presented in figure 16. In the upper left of the figure, the variation of the side-force coefficient c_y' developed at a flow incidence of 10° is presented as a function of Reynolds number, and the change in the direction of the side force that occurs at a Reynolds number of approximately 0.55×10^6 is clearly shown. In the upper right of the figure the theoretical pressure distribution obtained by the method of reference 4 is shown for a square cylinder having corner shapes almost identical (fig. 5) to those of the test square. It will be noted that rather large negative pressure loops are developed in the vicinity of the corners. However, for the conditions of the calculations (that is, potential flow with no circulation) there is, of course, no resultant force developed. In the lower part of figure 16 the experimental pressure distributions are shown for a subcritical and a supercritical Reynolds number (corresponding to the solid symbols on the side-force plot). At the subcritical Reynolds number, separation is observed to result in essential elimination of all the pressure loops except that associated with the right leading

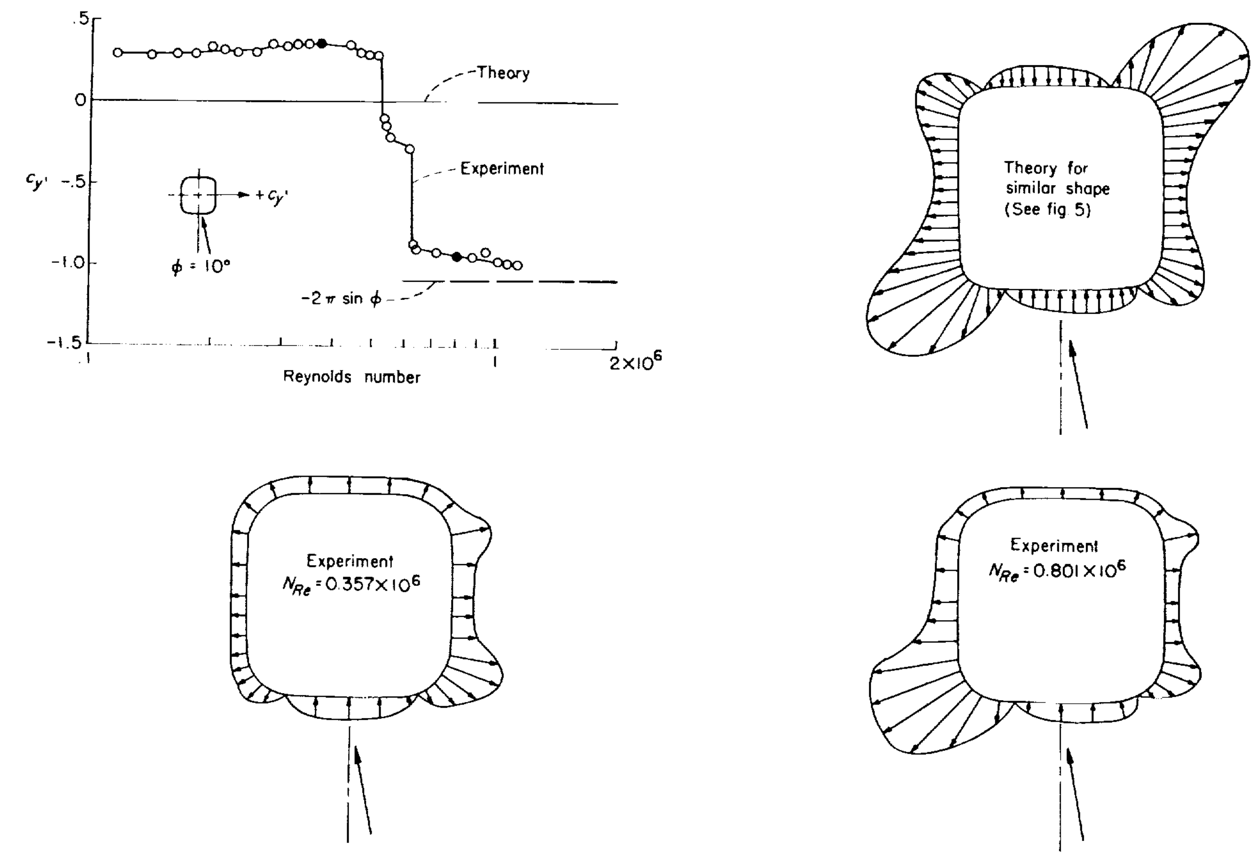

FIGURE 16.—Effect of Reynolds number on the side force and pressure distribution for a modified square cylinder at a flow incidence of 10°. $r/b_o=0.24$ (cylinder A); force data from reference 1.

corner. These losses are due to the large adverse gradients predicted by the theory and results in a positive overall side force as indicated by the side-force data. At the supercritical Reynolds number the large pressure loop on the left leading corner is produced and a large negative overall side force is developed. At supercritical Reynolds numbers the side force approaches that predicted for a flat plate having circulation sufficient to satisfy the Kutta condition at the trailing edge and is apparently associated with the fact that the flow about the cylinder at supercritical Reynolds numbers does not separate until the trailing corners are reached and the air is therefore deflected through the angle ϕ. It is possible, however, that at Reynolds numbers somewhat higher than were obtainable in the present investigation, flow attachment around the trailing corners might be maintained for a distance sufficient to develop the pressure loops predicted by theory to an extent such that the negative side force may be considerably reduced. An interesting phenomenon to be observed is the decrease in the pressure loop around the leading right corner with increasing Reynolds number. This phenomenon can possibly be explained by considering the movement of the stagnation point with changes in pressure distribution. For example, at the subcritical Reynolds number the large reduction in the pressure loop on the left leading corner would tend to move the stagnation point toward the plane of symmetry and thereby would cause the pressure loop on the right leading corner to approach in magnitude that for the zero flow incidence case which, of course, is larger than that predicted for the flow incidence of 10° (see table IX). Therefore, the pressure loop on the right leading corner would be expected to be larger than predicted by theory at subcritical Reynolds numbers and to approach the theoretical prediction in the supercritical Reynolds number range. To be kept in mind also is the fact that the theoretical cross-section contour in figure 16 is not identical to the experimental contour (fig. 5) and that therefore quantitative comparisons of the theoretical and experimental pressure distributions should not be made.

Figure 16 presented results for a flow incidence of 10° only. Some results for other flow incidences are presented in figure 17 for Reynolds numbers of 0.438×10^6 and 0.88×10^6. In the lower part of figure 17 the side-force coefficient is presented as a function of flow incidence for both Reynolds numbers, whereas in the upper part the experimental pressure distributions for both Reynolds

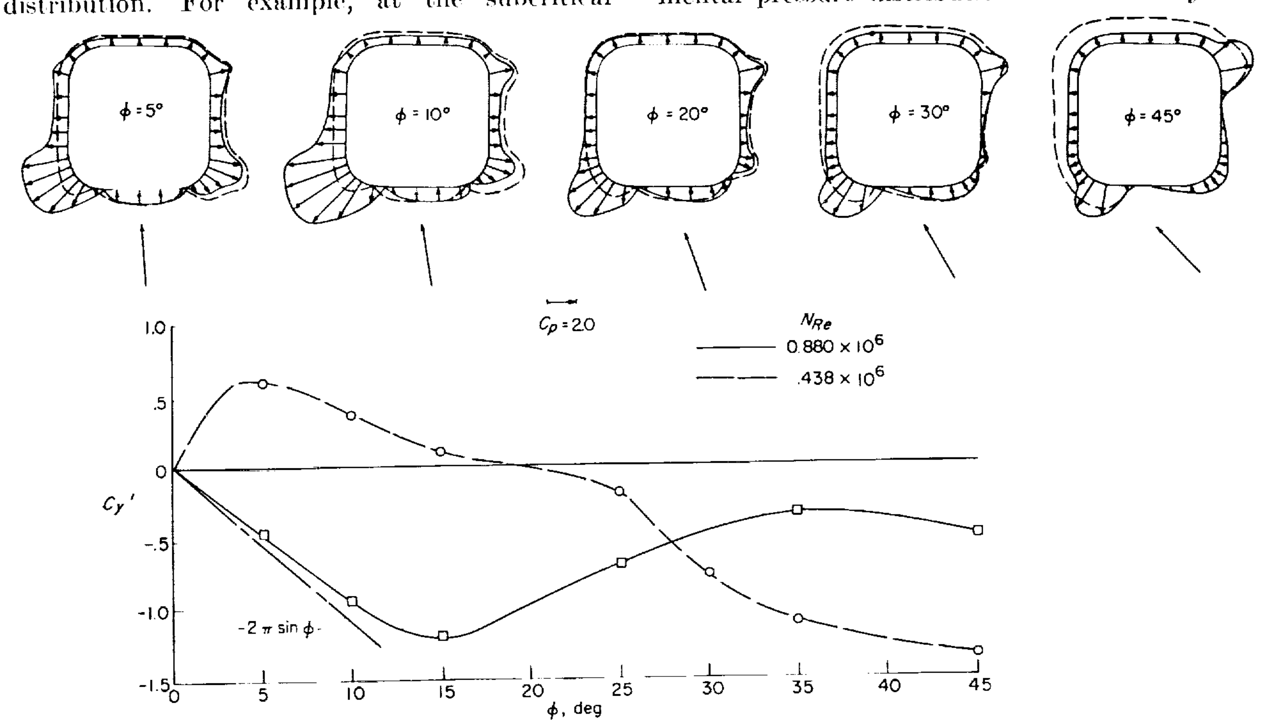

FIGURE 17.—Effect of flow incidence and Reynolds number on side force developed.

numbers and several flow incidences are presented. The results indicate that for flow incidences above 30°, the effect of Reynolds number is the reverse of that observed and discussed for the low incidence range. From the pressure distributions it can be seen that at the higher incidences the effect of Reynolds number on the face pressures is considerably greater than on the corner pressures and results in a reversal of the Reynolds number effect on side force relative to that observed at low incidences. The overall effects of Reynolds number and flow incidence on this square cylinder are quite similar to the effects of Reynolds number and rotational velocity on the Magnus effect of circular cylinders in the critical Reynolds number range. (See ref. 10.)

Also of interest in connection with the pressure distributions is the fact that for incidences below about 30° the reduction in c_x with increasing Reynolds number indicated in figure 4 of reference 1 appears to be associated as much with an increase in thrust on the windward face as with a decrease in drag on the leeward face.

Modified triangular cylinder.—Figure 18 presents results obtained for the modified triangular cylinder. The effect of Reynolds number is quite different from that observed for the modified square cylinder. At subcritical Reynolds numbers very little side force is developed, whereas at supercritical Reynolds numbers a rather large positive side force, which decreases with further increases in Reynolds number, is developed. From the theoretical pressure distributions, it can be seen that rather severe adverse pressure gradients are associated with the potential flow about both leading corners. The experimentally determined pressure distributions indicate that at low Reynolds numbers, the flow separates at both corners and a nearly symmetrical pressure distribution with a low value of side force results.

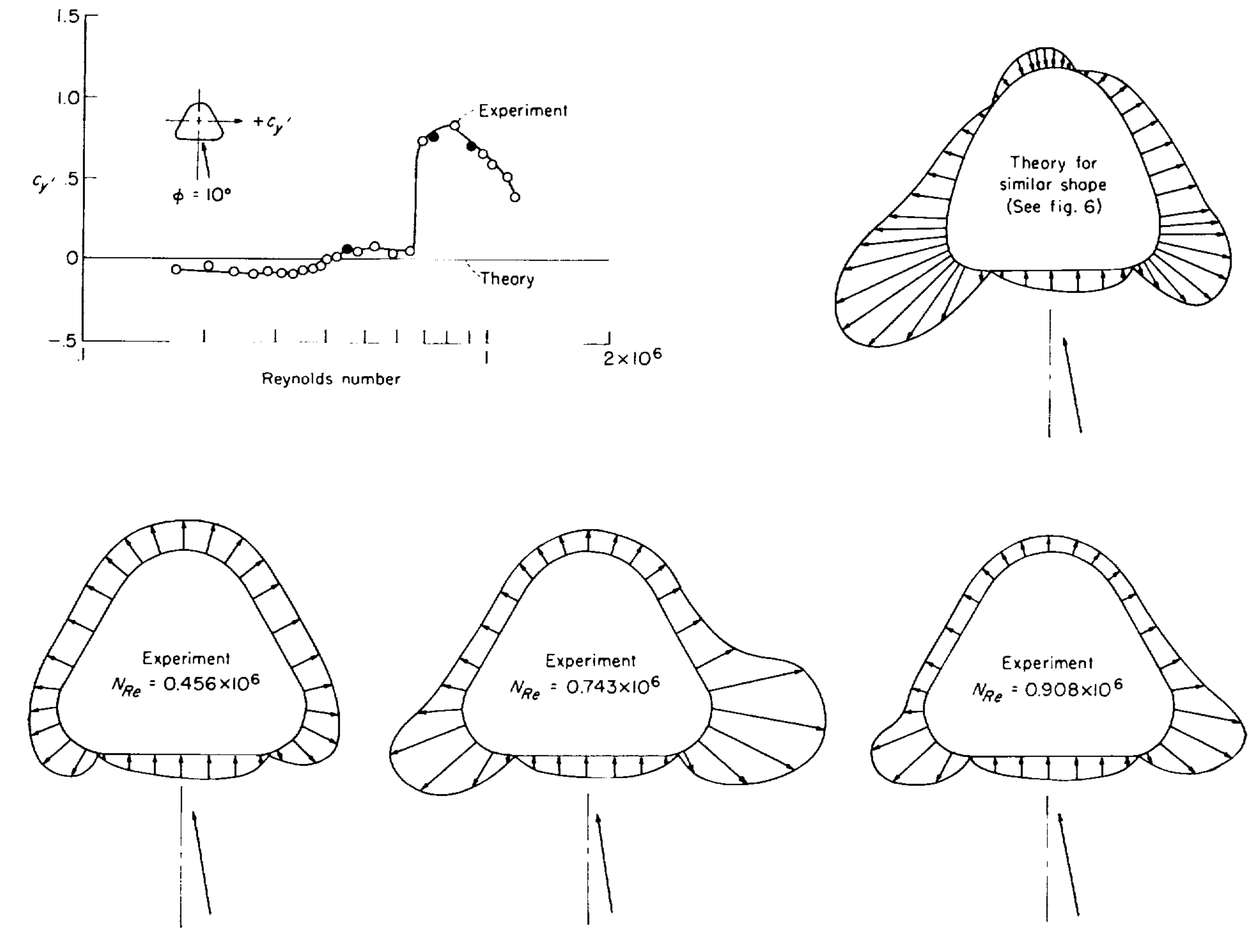

FIGURE 18.—Effect of Reynolds number on side force and pressure distribution for modified triangular cylinder at a flow incidence of 10°. (Coefficient based on c_o; force data from ref. 1.)

At a Reynolds number of 0.743×10^6 the pressure loops are considerably developed, with the loop associated with the right corner somewhat larger than the other so that a sizeable positive side force results.

The characteristics of the triangle in the inverted position are illustrated in figure 19. Large Reynolds number effects were again encountered with large negative side-force coefficients being developed at the lower Reynolds numbers but decreasing rather rapidly with increases in Reynolds numbers. The types of pressure distributions associated with these side forces are illustrated by the sketches.

Modified rectangular cylinders.—Figure 20 presents, for $\phi=10°$, the experimental side-force results and theoretical pressure distributions for two cross sections, both having a ratio of major to minor axis of 1.5 and almost identical leading corners. (See fig. 7.) Although the subcritical side-force characteristics and the critical Reynolds number are somewhat similar for the two cross sections, they are considerably different with regard to the supercritical side force developed, with the modified rectangular cross section experiencing a large negative side force as opposed to a small positive value for the more nearly triangular cross section. Experimental pressure distributions were not obtained for these particular cross sections; however, the potential-flow calculations offer a basis for a qualitative explanation of the differences observed. For example, the pressure distribution predicted for the rectangular cross section is, as would be expected, quite similar to that for the square cross section. (See fig. 16.) Therefore, the change in sign of the side force that occurs at a Reynolds number of about 0.51×10^6 would be expected, since separation similar to that discussed in connection with

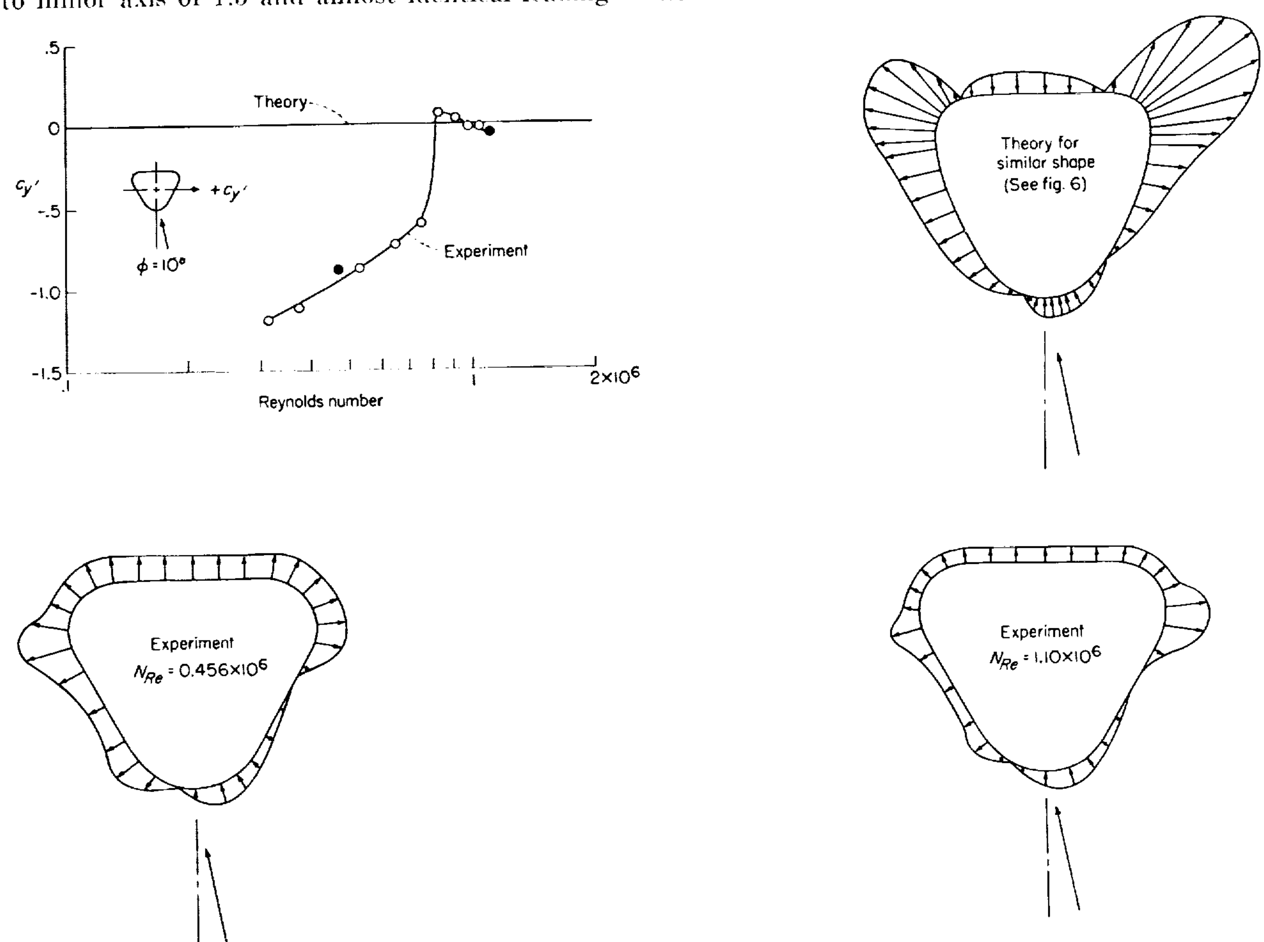

FIGURE 19.—Effect of Reynolds number on side force and pressure distribution for inverted modified triangular cylinder at a flow incidence of 10°. (Coefficients based on c_o.)

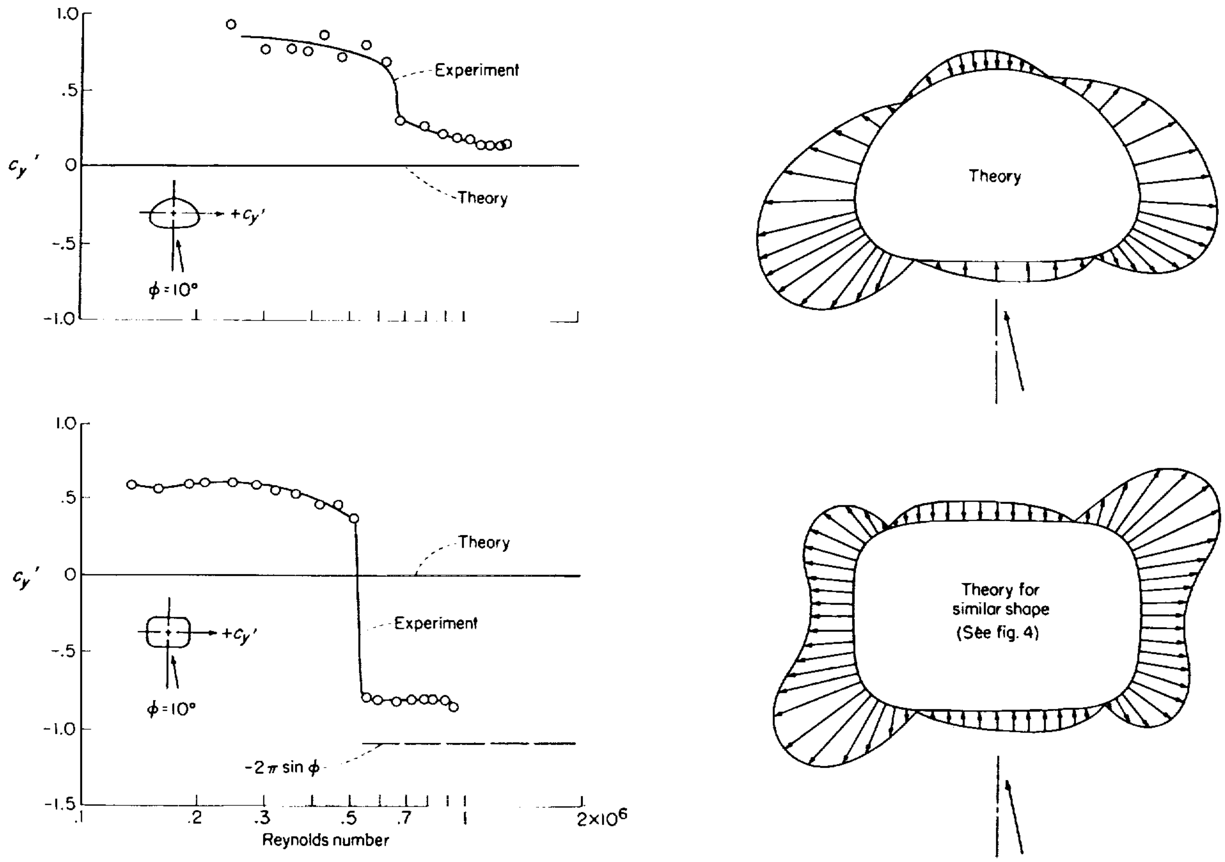

FIGURE 20.—Effect of Reynolds number and cross section on side force developed by cylinders at a flow incidence of 10°. (Coefficients based on c_o.)

the square cross section would be anticipated. For the more nearly triangular cross section (top of fig. 20) the number of negative pressure loops is, of course, reduced to two, each of which produces an almost equal (but opposite in direction) force. At Reynolds numbers below 2×10^5 little side force is developed, in all probability because of separation occurring at both leading corners as discussed in connection with the triangular shape shown in figure 18. As the Reynolds number increases, flow attachment occurs first on the right leading corner (due to the less severe adverse pressure gradient) and a rather large positive side force occurs. This flow attachment occurs at a considerably lower Reynolds number for this triangle than for the triangle of figure 18 since the corner radius is considerably larger and results in less adverse gradients. As the Reynolds number exceeds 6×10^5 the flow apparently attaches around the left leading corner and a reduction in the positive side force occurs. However, since the two potential-flow pressure loops would produce nearly equal forces (see fig. 20), no change in the sign of the side force would be expected as the left leading loop builds up with increasing Reynolds number. The difference in Reynolds number characteristics of the two cross sections therefore appears to be associated with the fact that for one, the two leading corner loops are of considerably different size while for the other they are nearly the same. At Reynolds numbers considerably higher than those obtained in this investigation it might be expected that the side force developed by both cross sections would approach zero. (See discussion of fig. 16.)

The experimental side force and theoretical pressure distributions for the elliptical cylinders at a flow incidence of 10° are presented in figure 21. The experimental side-force variation experienced by the ellipse having its major axis inclined 10° to the stream (top of fig. 21) is highly dependent upon Reynolds number. The negative side force developed decreases rather rapidly to a minimum as the Reynolds number increases to about

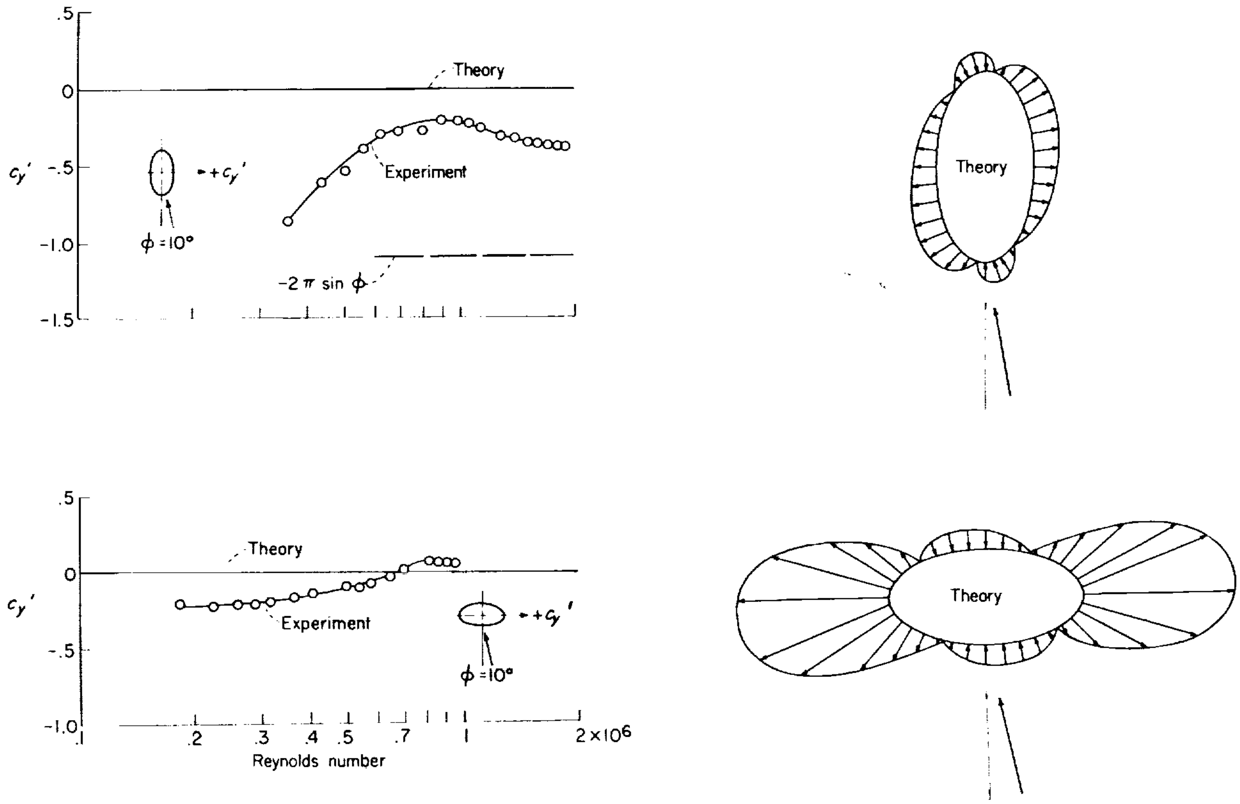

FIGURE 21.—Effect of Reynolds number and direction of major axis on the side force developed by elliptical cylinders of fineness ratio 2 at a flow incidence of 10°. (Coefficients based on c_o.)

0.80×10^6 above which a gradual increase in the negative side force occurs. Unfortunately, experimental pressure distributions are not available to substantiate and explain this large effect of Reynolds number. However, similar effects have been observed by other investigators in connection with studies of ellipses of higher fineness ratio (refs. 7 and 8) and some of their findings are presented in subsequent figures. The bottom part of figure 21 presents results for the ellipse with the minor axis inclined 10° to the stream and the effect of Reynolds number is seen to be considerably less than for the ellipse with the major axis inclined 10°. This result may be due to the fact that rather steep adverse pressure gradients exist on both corners and may cause the separation to occur at approximately the same location on both sides throughout the test Reynolds number range.

As stated previously, reference 7 contains results on an ellipse of considerably higher fineness ratio (fineness-ratio 6) that are somewhat similar to those of the present investigation and some of these results are presented in figures 22 and 23.

In figure 22 the variation of the side-force coefficient with Reynolds number for both the fineness-ratio-6 elliptical cylinder and an airfoil section (NACA 0018) having approximately the same thickness ratio is presented for flow incidences of 5° and 10°. The data for the airfoil section were obtained from reference 11. The results obtained for the elliptical cylinder are characterized by an initial decrease followed by an increase in the side force developed with increasing Reynolds number. However, the Reynolds number effect is considerably less extreme than that observed for the fineness-ratio-2 ellipse (fig. 21). For the NACA 0018 airfoil (fig. 22) the Reynolds number effect is limited to a very gradual increase with increasing Reynolds number. The difference in contour between the airfoil and the ellipse would indicate that the large Reynolds number effects indicated for the various elliptical cylinders are probably associated with the flow characteristics in the vicinity of the downstream stagnation point. For example, the pressure gradients around the downstream edge

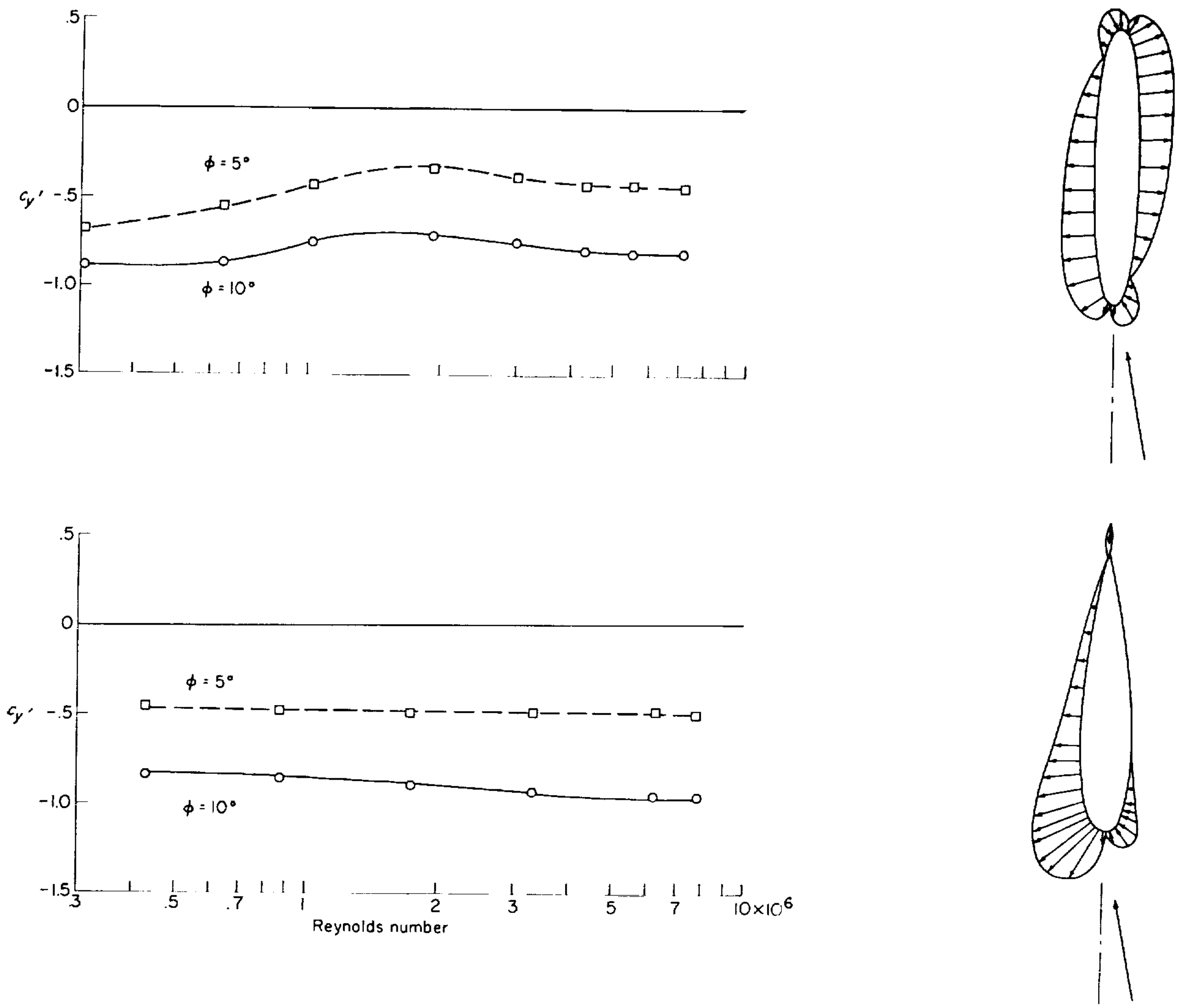

FIGURE 22.—Effect of Reynolds number and flow incidence on the side force developed on a fineness ratio 6 elliptic cylinder and an NACA 0018 airfoil section. (Data from refs. 7 and 11.) Note: Because of sharp trailing edge, circulation was included in airfoil pressure distribution.

of the fineness-ratio-2 ellipse (fig. 21) are apparently such that Reynolds number can have appreciable effect on the flow about the edge and considerable movement of the stagnation point and the accompanying variation in side force can occur. However, as the fineness ratio increases from 2 (fig. 21) to 6 (fig. 22), the adverse pressure gradients in the vicinity of the downstream stagnation point increase and probably limit the extent to which Reynolds number can affect the flow around the corner. For the airfoil section the sharp trailing edge assures a Kutta type of flow and the downstream stagnation point remains fixed at the trailing edge regardless of Reynolds number. Because of this condition the pressure distribution presented for the airfoil includes the circulation associated with the Kutta type of flow.

The results presented in figure 22 for the elliptic cylinder, although for only two angles of incidence, indicate considerable nonlinearity with incidence at the lower Reynolds numbers. This nonlinearity can be better seen in figure 23 where the side force is presented as a function of incidence for several Reynolds numbers. For Reynolds numbers of 1.94×10^6 and 7.21×10^6 the side force varies linearly with incidence up to about 10°, with a slight reduction in slope occurring beyond this incidence. At the two lower Reynolds

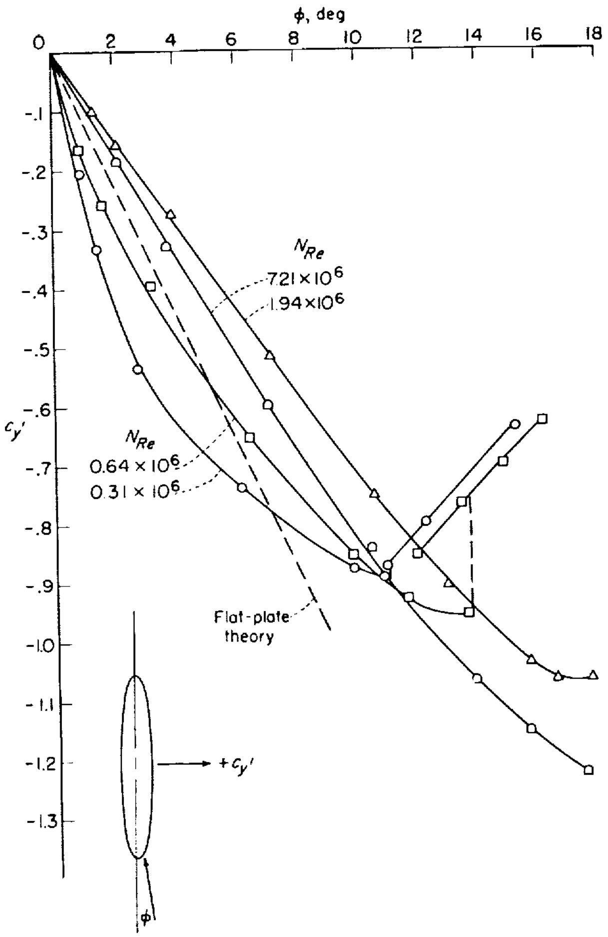

FIGURE 23.—Effect of Reynolds number on the variation of c_y' with ϕ for a 6 to 1 elliptic cylinder. (Data from ref. 7.)

numbers, however, the curves are considerably nonlinear, with that for the lowest Reynolds number having approximately twice the slope of a flat plate for incidences up to about 2° and approximately one-half the slope of a flat plate for incidences above about 4°.

Summary of theoretical results.—Figures 24 and 25 present the theoretical pressure distributions about several series of noncircular two-dimensional cylinders at a flow incidence of 10°. Those presented in figure 24 were determined by the method presented in appendix A, whereas those in figure 25 were determined by the method of reference 4. For certain flow conditions solutions are available for other shapes either in the tables herein or in references 4, 12, and 13, and these cross sections are shown in figure 26 with an indication of the particular flow condition and reference to the source of these solutions.

SPIN DAMPING BOUNDARY

In reference 1 it was shown that the side-force characteristics of two-dimensional cylinders could be used to predict the spin characteristics of fuselages, especially at large angles of attack such as those encountered in flat spins. For positive values of ϕ negative values of side force correspond to the condition of spin damping, and positive values correspond to a propelling condition. As was shown in figure 15 the side force developed on square cross sections is rather critically dependent upon Reynolds number and corner radius. Similar Reynolds number effects have been observed for rectangles. (See ref. 1.) Therefore, the tendency for square or rectangular fuselages to provide damping or propelling moments depends upon the Reynolds number and the corner radius. Figure 27 presents a probable boundary separating the damping conditions from the propelling conditions contributed by the fuselage as determined from figure 15 and reference 1. In this figure the boundary is presented as a function of the nondimensional corner radius and the Reynolds number based on the corner radius. Combinations of these two parameters which lie to the left of the cross-hatched boundary will probably result in the fuselage providing a propelling moment in a flat spin while those which lie to the right would be expected to provide damping. For values of r/b_o less than 0.37 the boundary was determined from the results presented in figure 15 for square cross sections and those of reference 1 for rectangles of fineness ratio 1.5. For values of r/b_o greater than 0.37, the boundary is based on the fact that damping would be expected at all Reynolds numbers for r/b_o of 0.5 (circle). In order to provide an indication of the Reynolds numbers associated with various combinations of velocity and corner radius, the variation of Reynolds number (based on corner radius) with velocity for corner radii of 1 foot and 0.1 foot are also shown for sea-level conditions. An indication of the effect of altitude is given for the 1-foot-radius condition.

It should be pointed out that the boundary presented in figure 27 should tend to be displaced to the left as the depth of the rectangle becomes sufficient to allow reattachment of the separated flow.

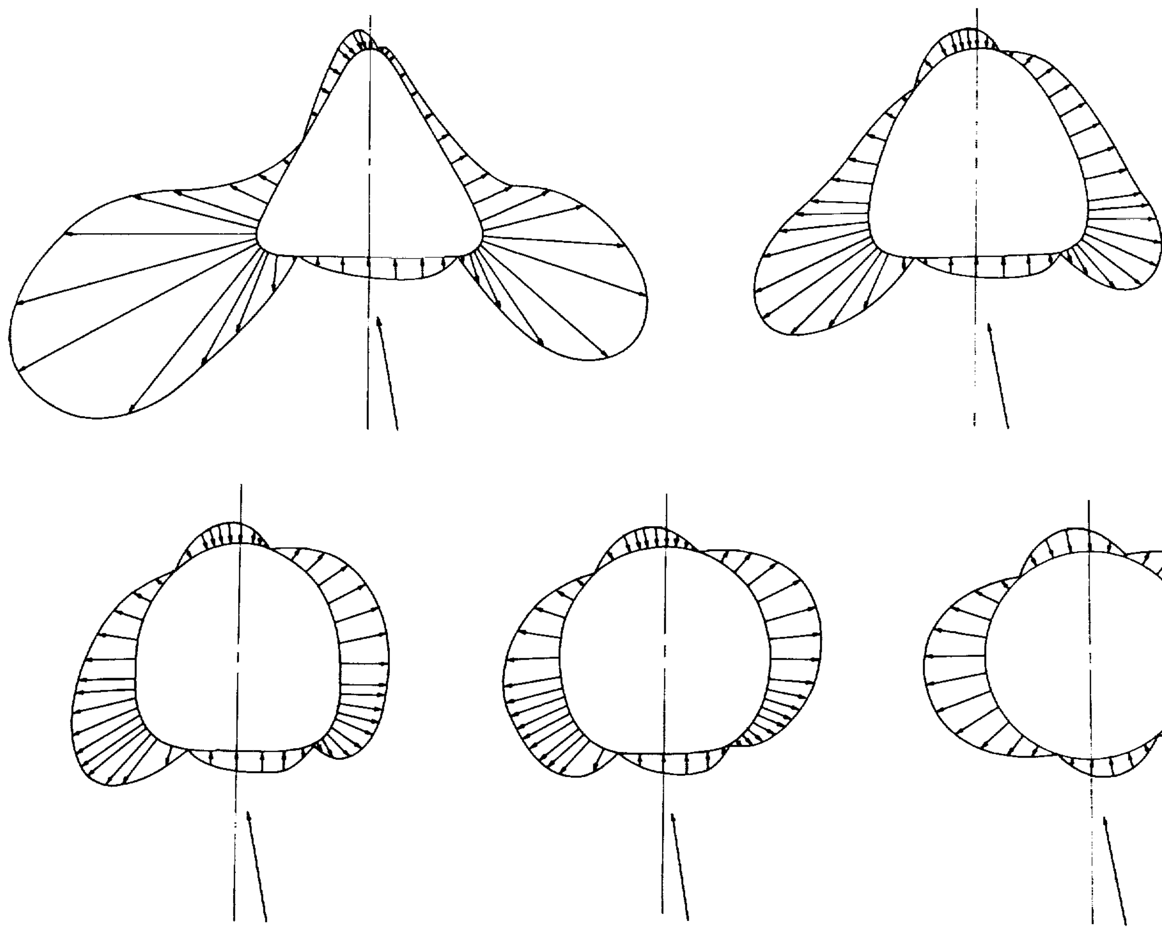

FIGURE 24.—Theoretical pressure distributions around a systematic series of cylinders ranging from a basically triangular cross section to a circular cross section. $\phi = 10°$.

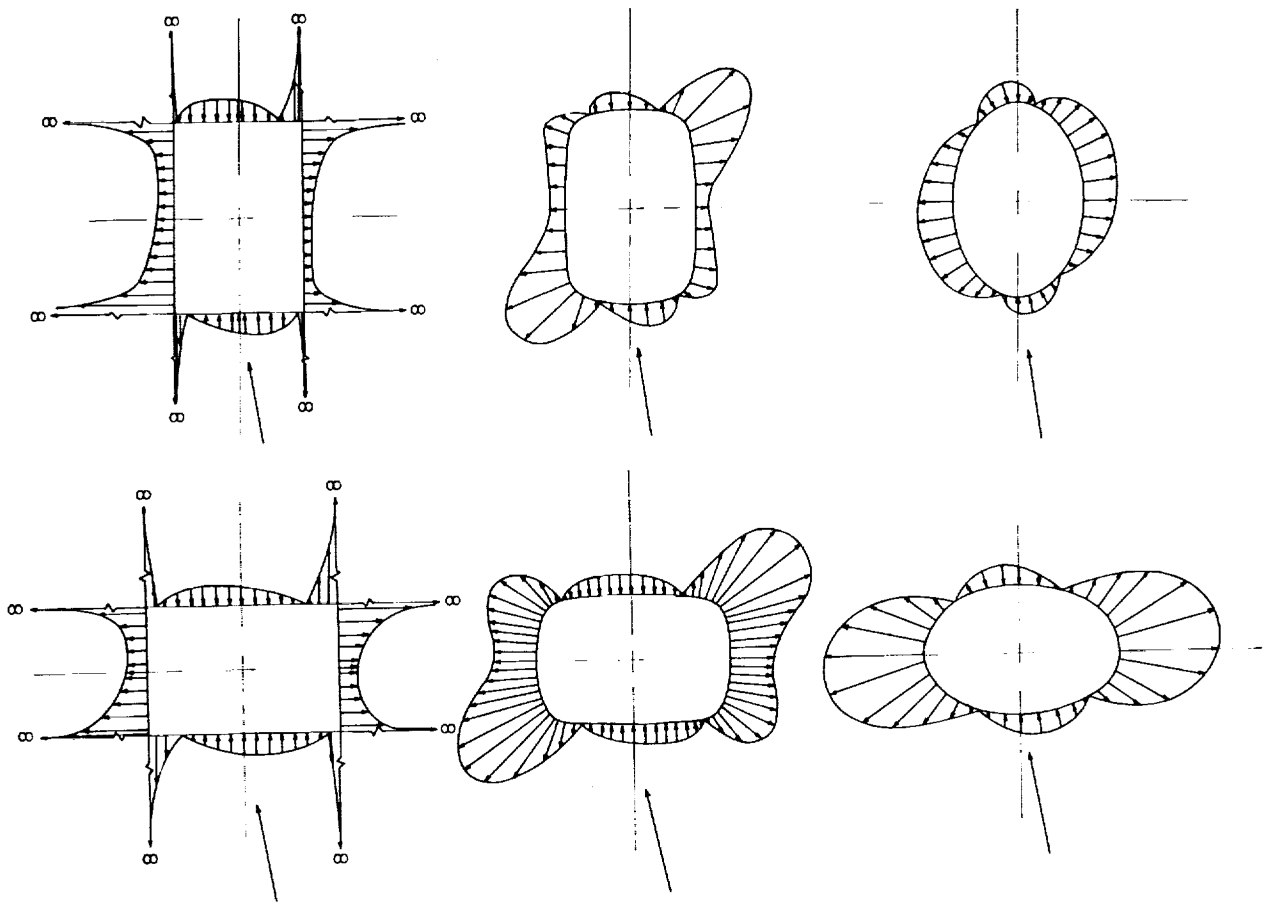

FIGURE 25.—Effect of surface curvature on the theoretical pressure distribution around several cylinders. $\phi=10$; $b_o/c_o=1.5$. (Method of ref. 4.)

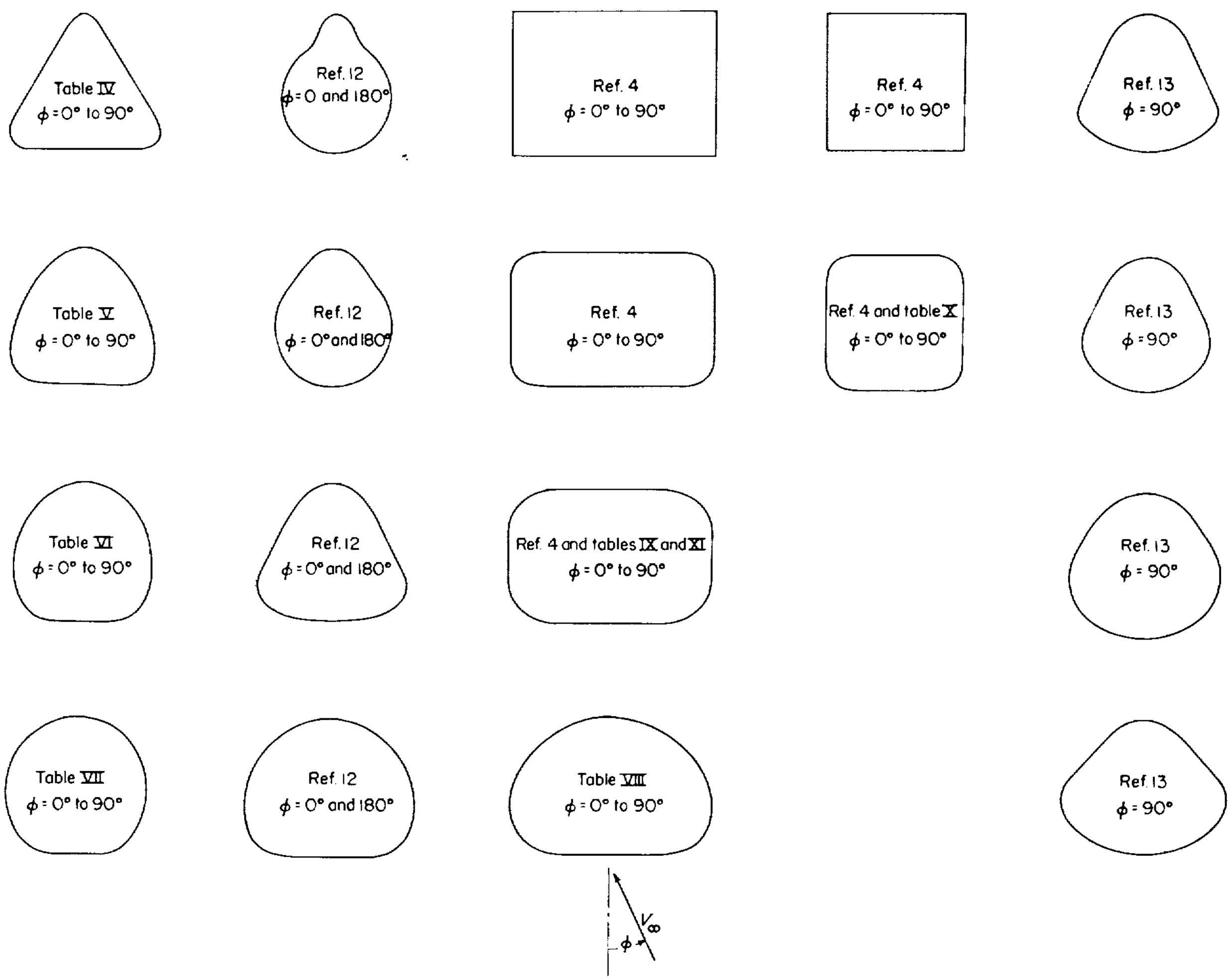

FIGURE 26.—Cross sections for which certain two-dimensional potential-flow solutions are available.

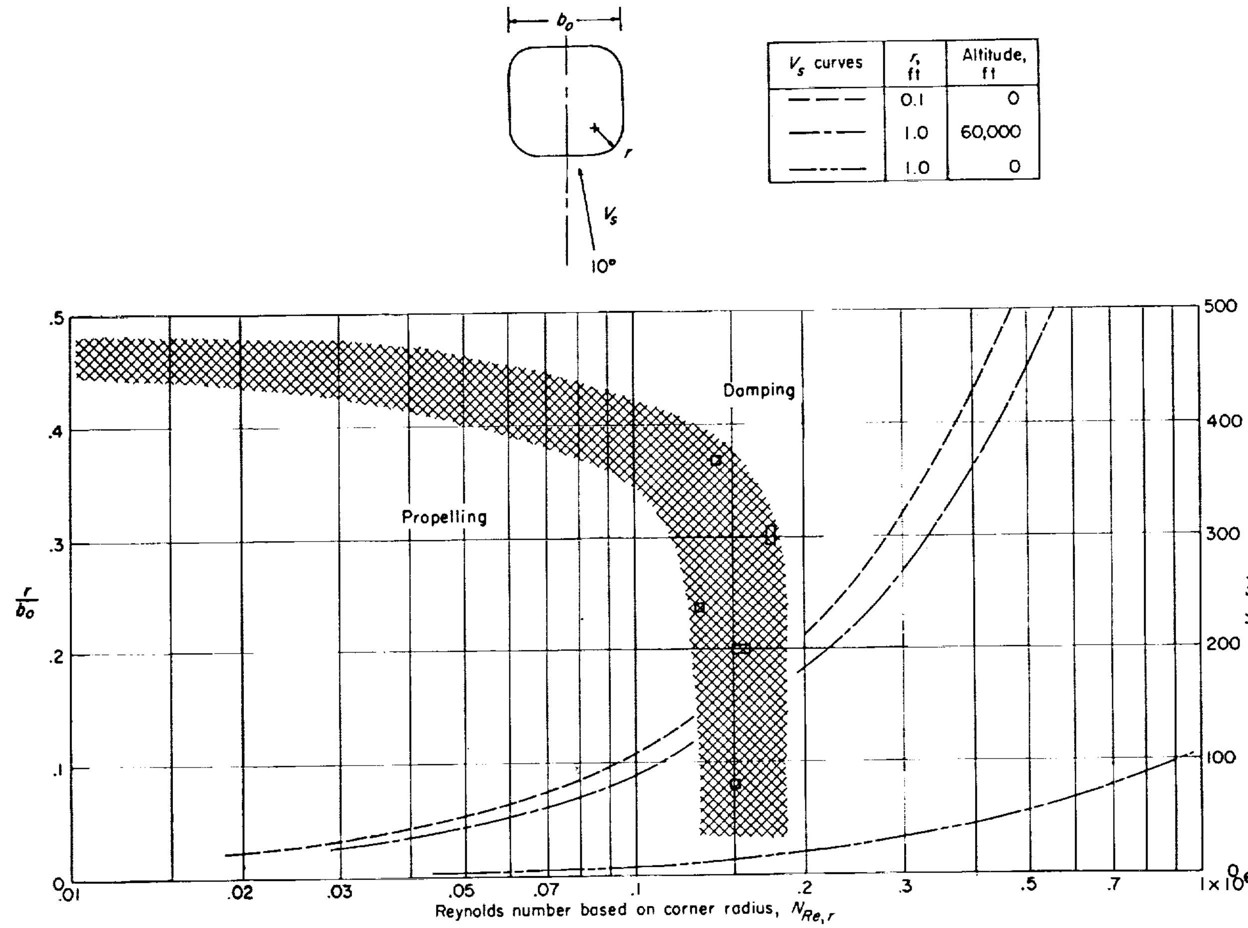

FIGURE 27.—Boundary between damping and propelling characteristics of square fuselages in flat spins.

CONCLUDING REMARKS

Low-speed wind-tunnel and theoretical studies have been made to determine the aerodynamic force and pressure-distribution characteristics of several noncircular two-dimensional cylinders normal to the airstream. The effect of Reynolds number, as well as the effect of flow incidence (obtained by rotating cylinder about its axis) for various elliptical and basically square and triangular cross sections, was investigated in the Reynolds number range from approximately 0.3×10^6 to 1.5×10^6.

All cross sections exhibited rather large Reynolds number effects, especially with regard to side force. The type of flow associated with the large variations in side force was determined for two of the cross sections by comparing the experimental and theoretical pressure distributions. With the knowledge thus obtained, it appears that the direction of the side force in various Reynolds number ranges can be predicted for other cross sections, provided the theoretical pressure distributions are available. For convenience in this respect, a method of determining the pressure distribution around arbitrary shapes is presented. It was found that, in addition to the pressure gradients encountered, the number of corners involved had appreciable influence on whether side-force reversals were encountered.

Of particular interest was the finding that the square cross section having corner radii of 37 percent of the cylinder depth develops, at supercritical Reynolds numbers, side forces that are approximately 62 percent of those developed by a flat plate, despite the fact that this cross section is closely approaching a circular (50 percent radius) cross section. Also in connection with this cross section it was found that at subcritical Reynolds numbers, the drag was actually lower than that of a circular cylinder by approximately 42 percent.

Inasmuch as the sinking speed and rotational velocity encountered by an aircraft in a flat spin provides flow incidences over the fuselage nose that are analogous to those of the present investigation, the side-force results were used to establish a boundary separating the probable propelling and damping characteristics.

Langley Research Center,
National Aeronautics and Space Administration,
Langley Field, Va., *Mar. 31, 1959.*

APPENDIX A

DETERMINATION OF PRESSURE DISTRIBUTION ABOUT THREE-CORNERED BODIES

This appendix contains a brief description of the method used for the determination of pressure distributions around a three-cornered body by use of ideal fluid-flow theory. The complex potential for the flow about a circle, as shown in sketch A-1, is given by

$$w=V_\infty \zeta e^{i\phi}+\frac{V_\infty R^2 e^{i\phi}}{\zeta-a} \tag{A1}$$

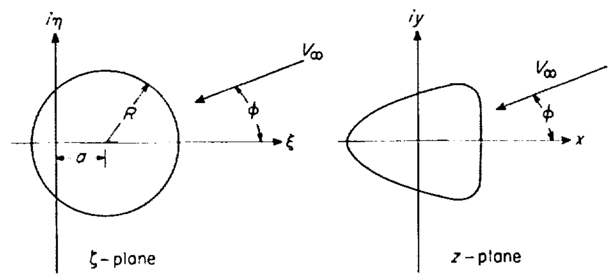

SKETCH A-1.

Points in the ζ-plane are transformed into points in the z-plane by the following relation derived in appendix B (eq. B-23):

$$z=\zeta-\frac{1-l^2}{\zeta}-\frac{l}{2}\frac{1}{\zeta^2} \tag{A2}$$

Such a transformation changes the circle in the ζ-plane into a contour with three rounded corners in the z-plane. The geometry of the shape into which the circle is transformed can be varied as explained in appendix B by varying the parameters R, a, and l. (See sketch B-3 of appendix B.)

The flow about this transformed contour is given by defining the complex potential w in the z-plane to be the same as for the corresponding points in the ζ-plane as given in equation (A1). The magnitude of the velocity is obtained from the complex potential according to, for the ζ-plane,

$$|V_\zeta|=\left|\frac{dw}{d\zeta}\right| \tag{A3}$$

and for the z-plane,

$$|V_z|=\left|\frac{dw}{dz}\right|$$

Thus, $|V_\zeta|$ and $|V_z|$ are related by

$$|V_z|=\frac{|V_\zeta|}{\left|\frac{dz}{d\zeta}\right|}$$

A similar expression relating the pressure coefficients in the z-plane to that for the corresponding point in the ζ-plane is obtained from the definition of C_p. Thus,

$$\frac{|V_z|^2}{V_\infty^2}=1-C_{p,z}$$

$$\frac{|V_\zeta|^2}{V_\infty^2}=1-C_{p,\zeta}$$

and with

$$|V_z|^2=\frac{|V_\zeta|^2}{\left|\frac{dz}{d\zeta}\right|^2}$$

then, by substitution,

$$1-C_{p,z}=\frac{1-C_{p,\zeta}}{\left|\frac{dz}{d\zeta}\right|^2}$$

or

$$C_{p,z}=1-\frac{1-C_{p,\zeta}}{\left|\frac{dz}{d\zeta}\right|^2}$$

$$=1+\frac{C_{p,\zeta}+1}{\left|\frac{dz}{d\zeta}\right|^2} \tag{A4}$$

From equation (A2),

$$\frac{dz}{d\zeta}=1+\frac{1-l^2}{\zeta^2}+\frac{l}{\zeta^3} \tag{A5}$$

Specifically then, if the pressure coefficient $C_{p,\zeta}$ at a particular point on the circle is known, the corresponding point on the transformed shape is found by equation (A2), and the pressure coefficient $C_{p,z}$ is given by equations (A4) and (A5).

It should be pointed out here that a general method applicable for arbitrary shapes is also described in appendix B.

APPENDIX B

A METHOD OF TRANSFORMING A CIRCLE INTO A DESIRED CROSS SECTION BY CONSIDERATION OF SINGULAR POINTS

TYPE OF TRANSFORMATION REQUIRED

The two-dimensional ideal fluid flow about a great variety of cross-sectional shapes can be obtained by a conformal transformation of the flow about a circle. Finding the equation $z=f(\zeta)$ that will transform a circle into a given shape can be facilitated by consideration of singular points.

The singular points of a transformation $z=f(\zeta)$ are those values of ζ for which $\frac{dz}{d\zeta}=0$. Thus, for example, the transformation

$$z=\zeta-\frac{1}{2}\frac{1}{\zeta^2}$$

has singular points at $\zeta=-1, e^{i\pi/3}, e^{-i\pi/3}$. Since

$$\frac{dz}{d\zeta}=1+\frac{1}{\zeta^3}=\left(1+\frac{1}{\zeta}\right)\left(1-\frac{e^{i\pi/3}}{\zeta}\right)\left(1-\frac{e^{-i\pi/3}}{\zeta}\right)$$

Application of this transformation to a circle ($|\zeta|=1$) passing through the three singular points produces a triangular-like shape with concave sides and three vertices corresponding to the three singular points as shown in sketch B–1:

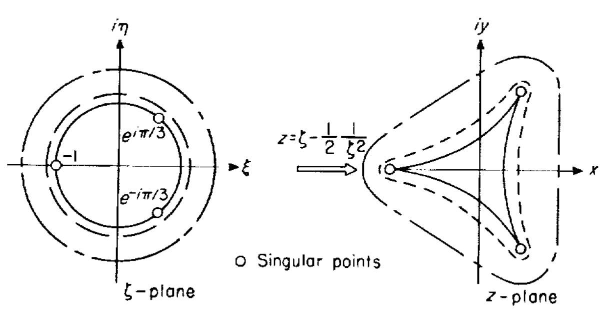

SKETCH B–1.

For a slightly larger circle not passing through the singular points, the shape in the z-plane has rounded corners instead of sharp vertices and the sides become less concave. Proper choice of circle radius will result in a shape with almost flat sections on each of the three sides as shown by the dash-dot curves in sketch B–1.

It is important to note that the closeness of the circle being transformed to the singular points in the ζ-plane determines the sharpness of the corners in the z-plane. Also, the number of singular points in the ζ-plane determines the number of corners in the z-plane.

Before a prescribed shape can be approximated, it is necessary to match other characteristics in addition to matching the number of rounded corners. Such details as curvature of the corners, length to width ratio, and flatness, convexity, or concavity of sides may be important. Although it is not apparent how to control all such variables independently, they can be manipulated to some extent by proper distribution of the singular points.

DEVELOPMENT OF TRANSFORMATION FUNCTION HAVING A GIVEN SET OF SINGULAR POINTS

The problem is to find a transformation $z=f(\zeta)$ that satisfies the following requirements:

(1) As ζ approaches ∞, the transformation approaches $z=\zeta$.

(2) Points for which $\frac{dz}{d\zeta}=0$ (singular points) occur at $\zeta=v_1, v_2, \ldots, v_n$.

The first requirement insures that a rectilinear flow at an infinite distance, in all directions from the origin in the ζ-plane, is unaltered by the transformation $z=f(\zeta)$. In order to satisfy this condition a transformation of the form

$$z=\zeta+\frac{b_1}{\zeta}+\frac{b_2}{\zeta^2}+\cdot\cdot\cdot+\frac{b_M}{\zeta^M} \qquad \text{(B1)}$$

is indicated. The constants $b_1, b_2, \ldots, b_M$ are to be chosen so that requirement 2 of the problem is satisfied. For this second requirement the expression for $\frac{dz}{d\zeta}$ must have n roots at $\zeta=v_1, v_2, \ldots, v_n$.

Thus

$$\frac{dz}{d\zeta}=1-\frac{b_1}{\zeta^2}-2\frac{b_2}{\zeta^3}-\cdot\cdot\cdot-M\frac{b_M}{\zeta^{M+1}}$$

$$=\left(1-\frac{v_1}{\zeta}\right)\left(1-\frac{v_2}{\zeta}\right)\cdot\cdot\cdot\left(1-\frac{v_n}{\zeta}\right) \qquad \text{(B2)}$$

The highest power of $\frac{1}{\zeta}$ resulting from the product of the n terms on the right-hand side is n. Hence $M+1=n$ and equation (B2) becomes

$$\frac{dz}{d\zeta}=1-\frac{b_1}{\zeta^2}-2\frac{b_2}{\zeta^3}-\cdot\cdot\cdot-(n-1)\frac{b_{n-1}}{\zeta^n}$$

$$=\left(1-\frac{v_1}{\zeta}\right)\left(1-\frac{v_2}{\zeta}\right)\cdot\cdot\cdot\left(1-\frac{v_n}{\zeta}\right) \qquad \text{(B3)}$$

The values of the constants $b_1,b_2, \ldots, b_{n-1}$ can be obtained in terms of the given singular point values $v_1,v_2 \ldots ,v_n$ by equating coefficients of like powers of $\frac{1}{\zeta}$ in equation (B3) after first expanding the right-hand side. Such an expansion gives

$$\left(1-\frac{v_1}{\zeta}\right)\left(1-\frac{v_2}{\zeta}\right)\left(1-\frac{v_3}{\zeta}\right)\cdot\cdot\cdot\left(1-\frac{v_n}{\zeta}\right)$$

$$=1-\frac{C_1}{\zeta}+\frac{C_2}{\zeta^2}-\cdot\cdot\cdot+(-1)^n\frac{C_n}{\zeta^n} \qquad \text{(B4)}$$

where

$$\left.\begin{aligned}
C_1&=v_1+v_2+\ldots+v_n\\
C_2&=(v_1v_2+v_1v_3+\ldots+v_1v_n)\\
&\quad+(v_2v_3+v_2v_4+\ldots+v_2v_n)+\ldots+(v_{n-1}v_n)\\
C_3&=(v_1v_2v_3+v_1v_2v_4+\ldots+v_1v_2v_n)+(v_1v_3v_4\\
&\quad+v_1v_3v_5+\ldots+v_1v_3v_n)+\ldots+(v_{n-2}v_{n-1}v_n)\\
&\ \ \vdots\\
C_n&=(v_1v_2v_3\ldots v_n)
\end{aligned}\right\} \qquad \text{(B5)}$$

Now equating coefficients of like powers of $\frac{1}{\zeta}$ in equation (B3) and equation (B4) yields

$$\begin{aligned}
0&=-C_1\\
-b_1&=C_2\\
-2b_2&=-C_3\\
-3b_3&=C_4\\
&\ \ \vdots\\
-(n-1)b_{n-1}&=(-1)^nC_n
\end{aligned}$$

and

$$\left.\begin{aligned}
&0=C_1=v_1+v_2+v_3+v_4\\
&b_1=-C_2=-[(v_1v_2+v_1v_3+\ldots\\
&\qquad\qquad+v_1v_n)+\ldots+(v_{n-1}v_n)]\\
&b_2=\frac{1}{2}C_3=\frac{1}{2}[(v_1v_2v_3+v_1v_2v_4+\ldots+v_1v_2v_n)\\
&\qquad\qquad+\ldots+(v_{n-2}v_{n-1}v_n)]\\
&b_3=-\frac{1}{3}C_4=-\frac{1}{3}[(v_1v_2v_3v_4+v_1v_2v_3v_5+\ldots\\
&\qquad\qquad+v_1v_2v_3v_n)+\ldots+(v_{n-3}v_{n-2}v_{n-1}v_n)]\\
&\quad\vdots\\
&b_{n-1}=b_M=\frac{(-1)^{n-1}}{(n-1)}C_n=\frac{(-1)^{n-1}}{n-1}\\
&\qquad\qquad(v_1v_2v_3\ldots v_n)
\end{aligned}\right\} \qquad \text{(B6)}$$

and the coefficients $b_1,b_2,\ldots,b_M$ are now evaluated in terms of the singular points $v_1,v_2,v_3,\ldots v_n$. Substituting equation (B6) into equation (B1) and remembering that $M=n-1$ yields the desired transformation.

It should be noted that in the attempt to find a solution of the form given in equation (B1), a restriction has been imposed upon the singular point distribution. The first relation of equation (B6) requires that

$$v_1+v_2+\ldots+v_n=0 \qquad \text{(B7)}$$

In other words, use of equation (B1) requires that the "centroid" of the singular point distribution be at the origin. This restriction is not serious, since the origin of the ζ-plane can be chosen to coincide with this centroid.

An expression which will be valid for any singular point distribution can be readily developed, as follows:

$$z=(\zeta-\mu)+\frac{b_1'}{(\zeta-\mu)}+\frac{b_2'}{(\zeta-\mu)^2}+\ldots+\frac{b_{n-1}'}{(\zeta-\mu)^{n-1}} \tag{B8}$$

where

$$\mu=\frac{v_1+v_2+v_3+v_4+\ldots+v_n}{n} \tag{B9}$$

$$\left.\begin{aligned}-b_1'&=(v_1'v_2'+v_1'v_3'+\ldots+v_1'v_n')+\ldots+(v_{n-1}'v_n')\\ 2b_2'&=(v_1'v_2'v_3'+v_1'v_2'v_4'+\ldots+v_1'v_2'v_n')+\ldots+(v_{n-2}'v_{n-1}'v_n')\\ &\;\;\vdots\\ \frac{(n-1)}{(-1)^{n-1}}b_{n-1}'&=(v_1'v_2'v_3'\ldots v_n')\end{aligned}\right\} \tag{B10}$$

and

$$\left.\begin{aligned}v_1'&=v_1-\mu\\ v_2'&=v_2-\mu\\ &\;\;\vdots\\ v_n'&=v_n-\mu\end{aligned}\right\} \tag{B11}$$

It is emphasized that the foregoing expressions are unnecessarily complicated for most cases. Usually, a more convenient approach is to choose the origin so that $\mu=0$, in which case equation (B8) reduces to equation (B1).

TRANSFORMATIONS WITH THREE SINGULAR POINTS AND AN AXIS OF SYMMETRY

Many fuselage cross sections are characterized by three "corners" (that is, three places where the curvature is a maximum). As a means of approximating such shapes, a three-singular-point transformation of a circle should first be tried. More exact approximations can be made by using more singular points; however, each added point produces another term in the transformation function.

The analysis to follow is concerned with the family of shapes that are obtained by transforming a circle by use of a transformation function with three singular points. If, furthermore, consideration is restricted to cases where the transformed shape is to have an axis of symmetry (a characteristic of most fuselage cross sections), then in the ζ-plane the circle to be transformed, together with the three singular points, must have a line of symmetry. If this line of symmetry is chosen to be the ξ-axis, and if the origin is chosen to be at the centroid of the singular point distribution (that is, chosen so that $v_1+v_2+\ldots+v_n=0$), the mathematics is then simplified and all possible transformed shapes subject to the preceding restrictions are obtained by varying the three parameters, a, $l(=2\cos\beta)$, and R shown in sketch B–2.

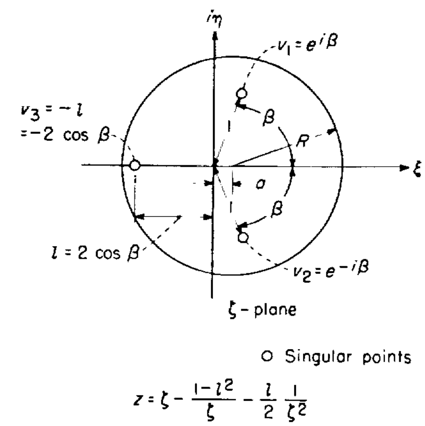

SKETCH B–2.

The proof that follows is offered in the interest of completeness and may be omitted through equation (B24) without loss of continuity, if desired.

Let the three singular points be

$$\left.\begin{aligned}v_1&=l_1e^{i\beta_1}\\ v_2&=l_2e^{i\beta_2}\\ v_3&=l_3e^{i\beta_3}\end{aligned}\right\} \tag{B12}$$

Inasmuch as the problem is concerned only with shapes, l_1 can be chosen to be unity. The following conditions are to be imposed:

(1) The origin is to be at the centroid of v_1, v_2, and v_3; that is,

$$\left.\begin{aligned}\mathscr{R}(v_1+v_2+v_3)=0\\ \mathscr{I}(v_1+v_2+v_3)=0\end{aligned}\right\} \tag{B13a}$$

(2) The singular points v_1, v_2, and v_3 have a line of symmetry coincident with the ξ-axis; that is,

$$\left.\begin{aligned}\mathscr{R}(v_1)&=\mathscr{R}(v_2)\\ \mathscr{I}(v_1)&=-\mathscr{I}(v_2)\\ \mathscr{I}(v_3)&=0\end{aligned}\right\} \tag{B13b}$$

It can be shown that

$$\beta_2=-\beta_1 \tag{B14}$$

$$l_2=l_1=1 \tag{B15}$$

or

$$\beta_3=0 \tag{B16}$$

$$l_3=-2\cos\beta_1 \tag{B17}$$

Thus the three singular points are

$$\left.\begin{aligned}v_1&=e^{i\beta_1}\\ v_2&=e^{-i\beta_1}\\ v_3&=-2\cos\beta_1\end{aligned}\right\} \tag{B18}$$

The subscripts on the l's may now be dropped. Also, for convenience in the following, let

$$l=2\cos\beta \tag{B19}$$

Then

$$\left.\begin{aligned}v_1&=e^{i\beta}\\ v_2&=e^{-i\beta}\\ v_3&=-2\cos\beta=-l\end{aligned}\right\} \tag{B20}$$

and the three singular points are located as shown in sketch B-2. It is emphasized that except for scale, equation (B20) and sketch B-2 represent all possible relative positions of three singular points with a line of symmetry. Only one parameter β (or l) is needed to define a particular arrangement.

The transformation function corresponding to the singular point distribution shown in sketch B-2 is given by equation (B1) to be

$$z=\zeta+\frac{b_1}{\zeta}+\frac{b_2}{\zeta^2} \tag{B21}$$

where, by equation (B6),

$$\left.\begin{aligned}-b_1&=v_1v_2+v_1v_3+v_2v_3\\ &=e^{i\beta}e^{-i\beta}+e^{i\beta}(-l)+e^{-i\beta}(-l)\\ &=1-l^2\\ 2b_2&=v_1v_2v_3\\ &=e^{i\beta}e^{-i\beta}(-l)\\ &=-l\end{aligned}\right\} \tag{B22}$$

Thus, the transformation is

$$z=\zeta-\frac{1-l^2}{\zeta}-\frac{l}{2}\frac{1}{\zeta^2} \tag{B23}$$

It is now necessary to consider all possible circles to be transformed by equation (B23). If symmetry about the ξ-axis is to be maintained, the center of the circle must be on the ξ-axis, and its position is therefore given by one coordinate a (the distance that the center is to the right of the origin, as shown in sketch B-2). The remaining parameter R defines the size of the circle. The equation of the circle is then

$$(\xi-a)^2+\eta^2=R^2 \tag{B24}$$

In summary, it has been shown that all possible shapes possessing a line of symmetry and obtainable from a circle transformed by a three-singular-point function of the form

$$z=\zeta+\frac{b_1}{\zeta}+\frac{b_2}{\zeta^2}$$

are given by varying the parameters l, a, and R where the circle (eq. (B24))

$$(\xi-a)^2+\eta^2=R^2$$

is transformed by (eq. (B23))

$$z=\zeta-\frac{1-l^2}{\zeta}-\frac{l}{2}\frac{1}{\zeta^2}$$

In a study of the family of shapes given by the preceding two equations, attention is first given to variation in the parameter R. Having chosen particular values for l and a, consider the subfamily of shapes in the z-plane obtained by varying R. A typical case is illustrated in sketch B–3.

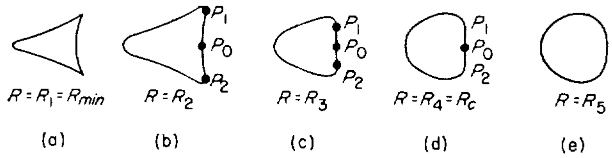

SKETCH B-3.—$a = -0.2$; $\beta = 60°$; $R_1<R_2<R_3<R_4<R_5$.

Note that:

(1) As R becomes large, the circle to be transformed is everywhere a large distance from the singular points and the transformed shape approaches a circle.

(2) The radius R can be decreased only until the circle passes through a singular point at which time the corresponding corner of the transformed shape becomes a sharp vertex (sketch B–3(a)). Further decrease in R would leave the singular point outside the circle and in the flow field that is also to be transformed to the z-plane.

The points P_0, P_1, and P_2 in sketch B–3 are points for which $\frac{dy}{dx}=\infty$. As R increases, P_1 and P_2 approach each other and at a certain value of R they meet at the point P_0 on the x-axis (sketch B–3(d)) and the shape is said to have a flat point. This critical value of R, herein designated R_c, may be obtained by the following quartic equation,

$$R_c^4+4aR_c^3+[6a^2-(1-l^2)]\,R_c^2+[4a^3-4a\,(1-l^2)-2l]\,R_c+[a^4-3a^2\,(1-l^2)+al]=0 \qquad \text{(B25)}$$

and is given by

$$R_c=\left(\sqrt[3]{f_1+\sqrt{f_2}}+\sqrt[3]{f_1-\sqrt{f_2}}-\frac{l^2-1}{6}\right)^{1/2}+2\left(\frac{\sqrt{f_3^2+f_4^2}-f_3}{2}\right)^{1/2}-a$$

where

$$f_1=(l^2-1)^3+54[a^2\,(l^2-1)^2+l^2]-216al\,(l^2-1)$$

$$f_2=\frac{1}{27648}\,[a^2\,(l^2-1)^5+(-5al+27a^4)\,(l^2-1)^4+(l^2-216a^3l)\,(l^2-1)^3+450a^2l^2\,(l^2-1)^2-216al^3\,(l^2-1)-432a^3l^3+27l^4]$$

$$f_3=\frac{\sqrt[3]{f_1+\sqrt{f_2}}+\sqrt[3]{f_1-\sqrt{f_2}}}{2}+\frac{l^2-1}{6}$$

$$f_4=\frac{\sqrt{3}}{2}\left(\sqrt[3]{f_1+\sqrt{f_2}}-\sqrt[3]{f_1-\sqrt{f_2}}\right)$$

The relation is developed as follows. Corresponding to $z=f(\zeta)$ or $(x+iy)=f(\zeta+i\eta)$, the real and imaginary parts can be equated to express the transformation in real variables:

$$x=f_1\,(\zeta,\eta)$$

$$y=f_2\,(\zeta,\eta)$$

Let $\eta=h[\zeta]$ be the equation of the curve to be transformed. Then

$$x=f_1\,(\zeta,h\,[\zeta])=g_1\,(\zeta)$$

$$y=f_2\,(\zeta,h\,[\zeta])=g_2\,(\zeta)$$

and the slope $\frac{dy}{dx}$ of the transformed curve is given by

$$\frac{dy}{dx}=\frac{dy/d\zeta}{dx/d\zeta}=\frac{g_2'(\zeta)}{g_1'(\zeta)}$$

The functions $g_1(\zeta)$ and $g_2(\zeta)$ are obtained from equations (B23) and (B24). Then it can be shown that the point P_0 (sketch B–3) corresponding to $\zeta=R+a$ satisfies the condition $g_2'(\zeta)=\infty$ and therefore has an infinite slope. The two other points having infinite slope in sketch B–3 correspond to the value of ζ satisfying $g_1'(\zeta)=0$ and will coincide with P_0 only if

$$g_1'\,(R+a)=0$$

Equation (B25) is the above relation with R designated as R_c.

For this critical condition $R=R_c$ the right side of the transformed shape most closely approximates a flat side. For values of R less than R_c, the right side has a concavity, and for values greater than R_c the right side is entirely convex. The other two sides are affected in the same manner by variation in R but do not necessarily reach the condition between concavity and convexity at the same value of R that produces this condition for the right side (see sketch B–3(c)).

The member of the subfamily obtained for $R=R_c$ is a shape from which the other members can be visualized, and this distinguishing member will be used in the following study. In other words, the family of shapes is reduced to a two-parameter family by not varying R independently but by determining it through equation (B25) after a and l are chosen.

THE TWO-PARAMETER (a, l) FAMILY

The effect of variation of the parameters a and l is shown in sketch B-4. The rows correspond to variation of a at constant value of l, whereas the columns correspond to variation of l (or β) at constant a.

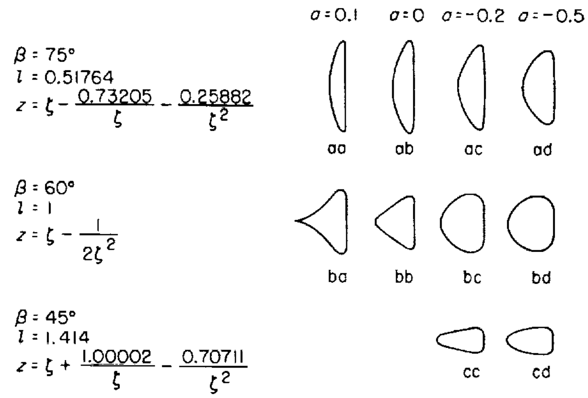

SKETCH B-4.

Several trends are displayed by sketch B-4. First as the parameter a increases negatively (that is, as the circle is shifted to the left), the ratio of height to width approaches unity as the shape approaches a circle. Conversely as a increases positively, the corners become sharper and the longest dimension increases relative to the shortest. Now, the ratio of height to width can also be changed by varying l (compare columns of sketch B-4). Thus a particular ratio can be attained by different combinations of a and l, each one giving different curvatures for the three corners. The prospect of matching a given shape is improved by the fact that ratio of width to height and relative curvature of the corners can be varied independently.

REFERENCES

1. Polhamus, Edward C.: Effect of Flow Incidence and Reynolds Number on Low-Speed Aerodynamic Characteristics of Several Noncircular Cylinders With Applications to Directional Stability and Spinning. NASA TR R-29, 1959. (Supersedes NACA TN 4176.)
2. Allen, H. Julian, and Vincenti, Walter G.: Wall Interference in a Two-Dimensional-Flow Wind Tunnel, With Consideration of the Effect of Compressibility. NACA Rep. 782, 1944.
3. Milne-Thomson, L. M.: Theoretical Hydrodynamics. Second ed., The Macmillan Co., 1950.
4. Maruhn, K.: Aerodynamische Untersuchungen an Rümpfen mit rechteckähnlichem Querschnitt. Jahrb. 1942 der deutschen Luftfahrtforschung, R. Oldenbourg (Munich), I 263–I 279. (Also available as NACA TM 1414, 1958.)
5. Delany, Noel K., and Sorensen, Norman E.: Low-Speed Drag of Cylinders of Various Shapes. NACA TN 3038, 1953.
6. Lindsey, W. F.: Drag of Cylinders of Simple Shapes. NACA Rep. 619, 1938.
7. Williams, D. H., and Brown, A. F.: Experiments on an Elliptic Cylinder in the Compressed Air Tunnel. R. & M. No. 1817, British A.R.C., 1937.
8. Warden, R.: Resistance of Certain Strut Forms. R. & M. No. 1599, British A.R.C., 1934.
9. Lanchester, F. W.: Aerodynamics. Fourth ed., Constable & Co., Ltd. (London), 1918.
10. Swanson, W. M.: An Experimental Investigation of the Two-Dimensional Magnus Effect. Contract No. DA-33-019-ORD-1434, Dept. Mech. Eng., Case Inst. Tech., Dec. 31, 1956. (Available from ASTIA as AD No. 122945.)
11. Abbott, Ira H., von Doenhoff, Albert E., and Stivers, Louis S., Jr.: Summary of Airfoil Data. NACA Rep. 824, 1945.
12. Liess, W., and Riegels, F.: Bemerkungen zum Rumpfeinfluss. Jahrb. 1942 der deutschen Luftfahrtforschung, R. Oldenbourg (Munich), pp. I 366–I 373.
13. Ksoll, R.: Theoretical Investigations on the Rolling Moment Due to Side Slip of Wing and Fuselage Arrangements With a Fuselage of Pear Shaped Cross Section. Reps. and Translations No. 134. British M. O. S. (A), Volkenrode.

TABLE I. PRESSURES MEASURED AROUND THE MODIFIED SQUARE CYLINDER

[Orifices numbered in clockwise direction (see fig. 8)]

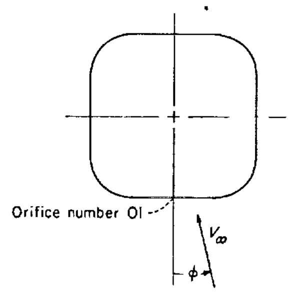

$\phi=0°$

Orifice	C_p for Reynolds number of:			
	303,000	438,000	620,000	878,000
01	.972	.971	.988	.995
02	.877	.867	.888	.890
03	.038	.012	.029	.022
04	−1.000	−1.121	−1.139	−1.153
05	−1.764	−2.104	−2.200	−2.244
06	−1.830	−2.592	−2.682	−2.734
07	−1.604	−2.654	−2.788	−2.856
08	−1.557	−2.463	−2.735	−2.791
09	−1.509	−1.271	−1.382	−1.395
10	−1.472	−1.008	−1.053	−1.060
11	−1.415	−.938	−.971	−.983
12	−1.245	−.971	−1.004	−1.020
13	−1.160	−1.283	−1.357	−1.363
14	−1.066	−.546	−.580	−.613
15	−1.019	−.554	−.590	−.635
16	−.943	−.550	−.592	−.635
17	−.925	−.550	−.592	−.640
18				
19	−1.057	−.546	−.592	−.631
20	−1.085	−.546	−.584	−.618
21	−1.151	−1.267	−1.351	−1.362
22	−1.226	−.938	−1.100	−1.000
23	−1.264	−.942	−1.065	−1.002
24	−1.264	−1.033	−1.100	−1.112
25	−1.255	−1.308	−1.422	−1.448
26	−1.264	−2.604	−2.892	−2.935
27	−1.311	−2.942	−3.280	−3.349
28	−1.453	−2.371	−2.514	−2.240
29	−1.321	−1.958	−2.069	−2.070
30	−.887	−1.288	−1.376	−1.373
31	.198	.029	.004	.012
32	.906	.862	.867	.868

$\phi=5°$

Orifice	C_p for Reynolds number of:				
	303,000	438,000	620,000	801,000	878,000
01	1.081	1.032	1.004	.965	.941
02	1.018	.903	.758	.724	.724
03	.261	.097	−.566	−.580	−.485
04	−.595	−.758	−2.052	−2.038	−1.859
05	−1.135	−1.258	−3.303	−3.255	−3.036
06	−.964	−1.000	−3.722	−3.666	−3.451
07	−.865	−.895	−3.699	−3.650	−3.450
08	−.892	−.778	−3.564	−3.443	−3.262
09	−.865	−.750	−1.764	−1.708	−1.613
10	−.874	−.758	−1.313	−1.258	−1.192
11	−.874	−.766	−1.163	−1.106	−1.054
12	−.883	−.770	−1.098	−1.043	−.997
13	−.883	−.790	−1.215	−1.138	−1.104
14	−.874	−.770	−.608	−.587	−.558
15	−.856	−.758	−.618	−.596	−.570
16	−.820	−.742	−.616	−.596	−.566
17	−.820	−.738	−.618	−.594	−.565
18					
19	−.811	−.726	−.610	−.594	−.561
20	−.802	−.738	−.608	−.586	−.557
21	−1.757	−1.714	−1.549	−1.474	−1.393
22	−1.342	−1.149	−.977	−.917	−.878
23	−1.306	−1.081	−.902	−.832	−.807
24	−1.387	−1.157	−.958	−.889	−.866
25	−1.829	−1.419	−1.192	−1.114	−1.098
26	−3.099	−2.726	−2.378	−2.250	−2.229
27	−3.586	−3.129	−2.666	−2.487	−2.476
28	−2.874	−2.363	−1.850	−1.530	−1.499
29	−2.360	−1.879	−1.370	−1.219	−1.246
30	−1.568	−1.161	−.699	−.579	−.623
31	.009	.177	.443	.480	.427
32	.973	.960	1.000	.979	.941

$\phi=10°$

Orifice	C_p for Reynolds number of:			
	303,000	438,000	620,000	801,000
01	.870	1.047	.926	.923
02	.757	.869	.685	.547
03	.009	−.072	−.571	−1.244
04	−.635	−.915	−1.831	−2.998
05	−.861	−1.297	−2.802	−4.390
06	−.687	−1.030	−3.023	−4.750
07	−.687	−1.000	−2.699	−4.574
08	−.670	−.924	−2.334	−4.154
09	−.670	−.903	−1.456	−2.060
10	−.670	−.898	−1.043	−1.491
11	−.670	−.924	−.915	−1.278
12	−.670	−.915	−.940	−1.118
13	−.696	−.941	−1.056	−1.031
14	−.687	−.924	−.965	−.616
15	−.670	−.911	−.940	−.628
16	−.652	−.877	−.829	−.629
17	−.635	−.873	−.790	−.627
18				
19	−.635	−.852	−.779	−.623
20	−.643	−.856	−.784	−.619
21	−1.557	−2.064	−1.885	−1.676
22	−1.000	−1.275	−1.082	−.890
23	−.870	−1.136	−.932	−.731
24	−.861	−1.178	−.961	−.741
25	−1.213	−1.352	−1.128	−.881
26	−1.852	−2.525	−2.150	−1.791
27	−2.183	−2.903	−2.384	−1.914
28	−1.574	−2.030	−1.565	−1.033
29	−1.165	−1.525	−1.068	−.628
30	−.591	−.792	−.458	−.033
31	.383	.424	.542	.791
32	.870	1.038	.975	1.049

$\phi=15°$

Orifice	C_p for Reynolds number of:			
	303,000	438,000	620,000	717,000
01	1.000	.918	.911	.733
02	.763	.668	.543	.270
03	−.351	−.414	−.972	−1.776
04	−1.193	−1.168	−2.463	−3.562
05	−1.246	−1.189	−3.461	−4.895
06	−1.096	−1.086	−3.519	−5.093
07	−1.105	−.980	−3.115	−4.766
08	−1.088	−.943	−2.438	−4.237
09	−1.079	−.930	−1.477	−2.081
10	−1.079	−.922	−1.154	−1.473
11	−1.088	−.906	−1.042	−1.221
12	−1.105	−.914	−1.046	−.994
13	−1.149	−.947	−1.028	−.783
14	−1.175	−.939	−1.028	−.542
15	−1.158	−.889	−1.008	−.556
16	−1.105	−.844	−.927	−.554
17	−1.088	−.828	−.893	−.551
18				
19	−1.044	−.820	−.883	−.547
20	−1.079	−.828	−.899	−.551
21	−2.500	−2.049	−2.188	−1.605
22	−1.351	−1.107	−1.117	−.725
23	−1.088	−.889	−.871	−.548
24	−1.053	−.885	−.848	−.490
25	−1.246	−.947	−.943	−.521
26	−2.044	−1.775	−1.780	−1.095
27	−2.351	−2.020	−1.915	−1.147
28	−1.482	−1.234	−1.059	−.432
29	−.974	−.783	−.568	−.037
30	−.281	−.172	.022	.414
31	.711	.684	.818	.913
32	1.096	.988	1.040	.951

TABLE I.—PRESSURES MEASURED AROUND THE MODIFIED SQUARE CYLINDER—Concluded

$\phi=20°$

Orifice	C_p for Reynolds number of:				
	303,000	438,000	620,000	717,000	878,000
01	.918	.844	.743	.797	.744
02	.564	.561	.362	.395	.317
03	-.818	-.561	-1.239	-1.278	-1.451
04	-1.709	-1.135	-2.443	-2.525	-2.631
05	-1.682	-.996	-3.126	-3.266	-3.243
06	-1.618	-.975	-2.907	-3.080	-2.724
07	-1.527	-.934	-2.532	-2.710	-1.478
08	-1.455	-.914	-1.783	-1.686	-1.165
09	-1.345	-.910	-1.261	-.950	-.887
10	-1.291	-.910	-.988	-.907	-.777
11	-1.255	-.906	-.917	-.859	-.763
12	-1.273	-.947	-.872	-.810	-.748
13	-1.300	-.992	-.885	-.810	-.772
14	-1.318	-1.016	-.872	-.819	-.748
15	-1.309	-.959	-.860	-.815	-.645
16	-1.264	-.906	-.804	-.798	-.623
17	-1.191	-.893	-.767	-.786	-.626
18					
19	-1.109	-.852	-.743	-.780	-.612
20	-1.236	-.885	-.769	-.804	-.612
21	-2.709	-2.184	-2.038	-2.070	-1.731
22	-1.327	-1.074	-.897	-.914	-.742
23	-.936	-.787	-.619	-.630	-.488
24	-.891	-.738	-.565	-.558	-.421
25	-1.027	-.762	-.585	-.598	-.447
26	-1.591	-1.402	-1.132	-1.188	-.969
27	-1.709	-1.557	-1.172	-1.202	-.926
28	-.836	-.783	-.449	-.437	-.195
29	-.373	-.352	-.055	-.015	.194
30	.200	.176	.383	.451	.609
31	.927	.828	.887	.961	1.002
32	1.055	.980	.933	.995	.969

$\phi=30°$

Orifice	C_p for Reynolds number of:				
	303,000	438,000	620,000	717,000	878,000
01	.486	.679	.579	.488	.500
02	.156	.265	.203	-.025	.018
03	-.917	-1.080	-1.108	-2.029	-1.851
04	-1.064	-1.189	-1.338	-3.155	-2.677
05	-1.028	-1.169	-1.176	-3.594	-2.702
06	-1.037	-1.129	-1.033	-3.071	-1.226
07	-1.046	-1.096	-.940	-1,935	-.860
08	-1.018	-1.096	-.927	-1.333	-.865
09	-1.064	-1.096	-.913	-1.070	-.794
10	-1.064	-1.120	-.911	-1.009	-.773
11	-1.092	-1.137	-.917	-.986	-.790
12	-1.183	-1.169	-.944	-.947	-.784
13	-1.275	-1.257	-.992	-.963	-.856
14	-1.339	-1.265	-.988	-.935	-.791
15	-1.376	-1.249	-.975	-.902	-.703
16	-1.229	-1.201	-.988	-.889	-.709
17	-1.156	-1.185	-.938	-.885	-.713
18					
19	-.982	-1.104	-.938	-.941	-.698
20	-.954	-1.161	-1.037	-1.022	-.689
21	-1.073	-1.618	-1.900	-1.780	-1.883
22	-.468	-.687	-.680	-.611	-.654
23	-.229	-.357	-.340	-.276	-.295
24	-.156	-.241	-.228	-.161	-.175
25	-.110	-.221	-.199	-.115	-.117
26	-.312	-.510	-.450	-.337	-.345
27	-.220	-.382	-.336	-.193	-.188
28	.266	.257	.249	.382	.386
29	.505	.606	.556	.656	.669
30	.752	.912	.815	.899	.905
31	.853	1.076	.952	.971	.974
32	.734	.936	.822	.780	.785

$\phi=45°$

Orifice	C_p for Reynolds number of:					
	303,000	438,000	620,000	717,000	878,000	1,017,000
01	.193	.159	.169	-.054	.096	.085
02	-.321	-.322	-.244	-.541	-.378	-.431
03	-1.807	-1.815	-1.576	-2.683	-2.157	-2.404
04	-1.569	-1.592	-1.393	-2.977	-2.254	-2.495
05	-1.550	-1.481	-1.206	-1.950	-.954	-1.167
06	-1.532	-1.481	-1.102	-1.061	-.731	-.933
07	-1.550	-1.506	-1.041	-.980	-.726	-.892
08	-1.615	-1.511	-1.081	-.940	-.678	-.839
09	-1.615	-1.558	-1.024	-.893	-.642	-.794
10	-1.661	-1.601	-1.033	-.875	-.646	-.798
11	-1.780	-1.652	-1.022	-.873	-.653	-.814
12	-1.817	-1.760	-.998	-.870	-.673	-.839
13	-2.028	-1.966	-1.006	-.878	-.689	-.862
14	-2.073	-2.026	-1.024	-.855	-.623	-.773
15	-2.119	-1.970	-1.020	-.852	-.650	-.826
16	-1.881	-1.768	-1.004	-.849	-.663	-.838
17	-1.771	-1.670	-1.006	-.841	-.651	-.811
18						
19	-1.596	-1.494	-1.047	-.992	-.714	-.868
20	-1.523	-1.558	-1.234	-1.476	-1.655	-1.431
21	-1.862	-1.880	-1.576	-1.680	-2.239	-2.447
22	-.358	-.386	-.238	-.202	-.457	-.504
23	.101	.120	.171	.232	.035	.029
24	.321	.309	.340	.405	.220	.234
25	.514	.498	.464	.549	.368	.393
26	.569	.554	.527	.631	.426	.452
27	.798	.760	.709	.803	.622	.675
28	1.092	1.060	.941	.994	.895	.967
29	1.156	1.133	1.002	1.012	.971	1.045
30	1.083	1.052	.941	.876	.920	.979
31	.725	.704	.625	.482	.617	.641
32	.486	.489	.432	.283	.388	.407

TABLE II.—PRESSURES MEASURED AROUND THE MODIFIED TRIANGULAR CYLINDER

[Orifices numbered in clockwise direction (see fig. 8)]

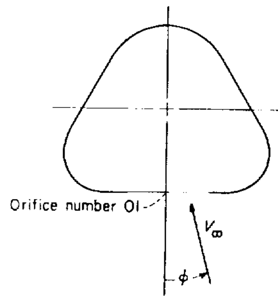

$\phi=0°$

Orifice	C_p for Reynolds number of:			
	311,000	456,000	743,000	901,000
01	.824	1.109	1.000	.979
02	.748	1.070	.952	.946
03	.664	.903	.787	.802
04		.213	.126	.202
05	−.639	−1.205	−1.301	−1.104
06	−1.353	−2.453	−2.764	−2.445
07	−1.353	−2.651	−3.525	−3.052
08	−1.244	−2.209	−2.658	−1.688
09	−1.118	−1.523	−1.023	−.925
10	−1.067	−1.384	−.956	−.851
11	−1.042	−1.376	−.928	−.820
12	−1.034	−1.310	−.933	−.816
13	−1.118	−1.357	−.943	−.841
14	−1.084	−1.295	−.926	−.812
15	−1.067	−1.302	−.877	−.773
16	−1.025	−1.275	−.863	−.758
17	−1.017	−1.271	−.906	−.792
18	−1.034	−1.295	−.954	−.834
19	−1.059	−1.326	−.986	−.860
20	−1.008	−1.322	−.975	−.839
21	−.992	−1.395	−.980	−.841
22	−.983	−1.399	−1.029	−.868
23	−1.034	−1.481	−1.126	−.912
24	−1.118	−2.031	−1.862	−.996
25	−1.218	−2.585	−3.166	−2.477
26	−1.294	−2.426	−2.721	−2.373
27	−.605	−1.155	−1.261	−1.095
28	.244	.217	.113	.158
29	.681	.915	.794	.793
30	.807	1.093	.960	.945

$\phi=10°$

Orifice	C_p for Reynolds number of:		
	456,000	743,000	901,000
01	1.036	1.076	1.015
02	.956	.947	.908
03	.698	.661	.665
04	−.052	−.317	−.163
05	−1.464	−2.121	−1.710
06	−1.976	−3.593	−2.914
07	−1.579	−3.865	−2.868
08	−1.429	−2.209	−.941
09	−1.444	−1.130	−.756
10	−1.440	−.963	−.710
11	−1.468	−.926	−.713
12	−1.488	−.944	−.724
13	−1.504	−.937	−.736
14	−1.480	−.935	−.706
15	−1.484	−.937	−.693
16	−1.556	−.946	−.717
17	−1.639	−.938	−.767
18	−1.651	−.935	−.804
19	−1.619	−1.263	−.838
20	−1.571	−1.221	−.837
21	−1.528	−1.316	−.912
22	−1.488	−2.025	−1.157
23	−1.500	−4.686	−1.697
24	−1.651	−5.958	−3.517
25	−2.036	−4.802	−3.433
26	−1.806	−3.172	−2.382
27	−.476	−1.025	−.698
28	.579	.437	.488
29	1.020	1.003	.962
30	1.079	1.098	1.033

$\phi=30°$

Orifice	C_p for Reynolds number of:		
	456,000	743,000	901,000
01	.823	.782	.711
02	.662	.555	.504
03	.357	.175	.121
04	−.523	−1.012	−1.003
05	−1.617	−2.690	−2.592
06	−1.553	−3.221	−2.968
07	−1.162	−1.905	−1.162
08	−1.023	−.897	−.680
09	−.970	−.805	−.631
10	−.959	−.756	−.602
11	−.966	−.740	−.589
12	−.970	−.742	−.590
13	−.962	−.731	−.589
14	−.962	−.722	−.584
15	−.940	−.720	−.580
16	−.910	−.724	−.578
17	−.887	−.717	−.577
18	−.932	−.733	−.587
19	−1.786	−1.485	−1.247
20	−1.564	−1.329	−1.123
21	−1.455	−1.284	−1.079
22	−1.876	−1.694	−1.445
23	−3.925	−3.737	−3.220
24	−4.139	−3.876	−3.328
25	−2.647	−2.389	−1.948
26	−1.113	−.888	−.596
27	.282	.442	.543
28	.914	.965	.946
29	1.008	1.012	.955
30	.970	.928	.860

$\phi=50°$

Orifice	C_p for Reynolds number of:		
	456,000	743,000	901,000
01	.333	.139	.160
02	.114	−.119	−.084
03	−.259	−.565	−.503
04	−1.271	−1.867	−1.715
05	−1.675	−3.095	−2.691
06	−1.345	−2.143	−1.100
07	−1.141	−.812	−.805
08	−1.090	−.748	−.756
09	−1.118	−.736	−.726
10	−1.086	−.724	−.698
11	−1.043	−.712	−.687
12	−1.024	−.697	−.671
13	−1.047	−.700	−.678
14	−1.043	−.706	−.675
15	−1.024	−.700	−.678
16	−.992	−.699	−.673
17	−.976	−.691	−.671
18	−1.549	−1.014	−.887
19	−2.443	−1.857	−1.784
20	−1.416	−1.041	−1.008
21	−.937	−.623	−.599
22	−.835	−.532	−.517
23	−1.510	−1.042	−1.031
24	−1.122	−.622	−.600
25	.082	.352	.382
26	.867	.902	.928
27	1.035	.905	.915
28	.839	.664	.665
29	.682	.518	.523
30	.522	.349	.361

$\phi=70°$

Orifice	C_p for Reynolds number of:		
	456,000	743,000	901,000
01	−.588	−.239	−.268
02	−.776	−.369	−.383
03	−1.139	−.607	−.621
04	−2.286	−1.316	−1.315
05	−2.502	−1.178	−1.061
06	−1.086	−.539	−.546
07	−1.078	−.551	−.554
08	−1.082	−.530	−.564
09	−1.073	−.520	−.557
10	−1.086	−.544	−.546
11	−1.110	−.539	−.555
12	−1.188	−.536	−.573
13	−1.273	−.512	−.603
14	−1.343	−.538	−.612
15	−1.388	−.533	−.628
16	−1.873	−.494	−.671
17	−3.437	−1.021	−.736
18	−3.686	−2.306	−2.021
19	−2.980	−2.142	−1.992
20	−1.041	−.779	−.694
21	−.118	−.116	−.057
22	.327	.215	.268
23	.482	.286	.364
24	.951	.744	.784
25	1.086	.955	.962
26	.514	.630	.604
27	−.588	−.134	−.199
28	−.796	−.318	−.380
29	−.371	−.072	−.115
30	−.453	−.143	−.169

TABLE III.—PRESSURES MEASURED AROUND THE INVERTED MODIFIED TRIANGULAR CYLINDER

Orifices numbered in clockwise direction (see fig. 8)]

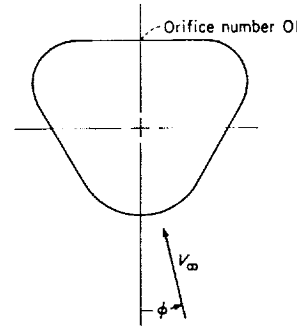

$\phi=0°$

Orifice	C_p for Reynolds number of:			
		743,000	901,000	1,046,000
01		−.901	−.763	−.640
02		−.898	−.769	−.650
03		−.903	−.777	−.664
04		−.922	−.799	−.699
05		−.934	−.821	−.724
06		− 972	−.845	−.723
07		−1.044	−.919	−.771
08		−1.704	−1.617	−1.075
09		−2.055	−2.112	−2.030
10		−.792	−.754	−.767
11		−.307	−.266	−.298
12		−.149	−.103	−.152
13		−.133	−.054	−.142
14		.343	.389	.342
15		.828	.847	.837
16		.981	.985	1.002
17		.781	.755	.802
18		.330	.271	.339
19		−.196	−.273	−.200
20		−.183	−.229	−.174
21		−.340	−.368	−.308
22		−.768	−.790	−.702
23		−1.939	−1.966	−1.754
24		−1.789	−1.306	−.864
25		−1.019	−.857	−.732
26		−.981	−.842	−.726
27		−.951	−.836	−.724
28		−.930	−.810	−.695
29		−.914	−.783	−.659
30		−.905	−.765	−.642

$\phi=10°$

Orifice	C_p for Reynolds number of:			
	456,000	743,000	901,000	1,046,000
01	−.996	−.953	−.748	−.667
02	−1.000	−.956	−.760	−.670
03	−1.024	−.965	−.767	−.680
04	−1.016	−.982	−.791	−.699
05	−1.004	−1.003	−.801	−.709
06	−1.012	−1.055	−.823	−.731
07	−1.091	−1.170	−.849	−.776
08	−1.256	−2.381	−2.408	−1.953
09	−1.260	−2.146	−2.249	−1.995
10	−.228	−.544	−.631	−.547
11	.205	.027	−.043	.009
12	.453	.322	.249	.270
13	.646	.517	.437	.434
14	.917	.874	.436	.423
15	.969	.997	.458	.207
16	.654	.772	.794	.480
17	.059	.152	.269	.291
18	−.642	−.538	−.379	−.331
19	−1.165	−1.153	−.913	−.857
20	−.862	−.754	−.581	−.854
21	−.760	−.739	−.570	−.526
22	−1.071	−1.058	−.852	−.776
23	−2.169	−2.119	−1.761	−1.581
24	−1.520	−1.179	−.880	−.733
25	−.933	−.939	−.742	−.653
26	−.941	−.951	−.751	−.658
27	−.969	−.959	−.759	−.667
28	−.996	−.951	−.752	−.663
29	−.984	−.945	−.748	−.658
30	−.988	−.953	−.726	−.664

$\phi=20°$

Orifice	C_p for Reynolds number of:			
	456,000	743,000	901,000	1,046,000
01	−1.016	−.772	−.697	−.662
02	−1.063	−.774	−.704	−.666
03	−1.063	−.784	−.708	−.673
04	−1.063	−.802	−.724	−.691
05	−1.071	−.821	−.726	−.694
06	−1.179	−.848	−.740	−.701
07	−1.437	−.950	−.779	−.725
08	−1.742	−2.847	−2.509	−2.362
09	−1.373	−2.065	−1.860	−1.770
10	−.012	−.348	−.288	−.234
11	.488	.305	.315	.351
12	.147	.629	.632	.658
13	−.857	.874	.838	.864
14	−1.456	.874	.996	.999
15	−1.504	.877	.832	.807
16	.020	.295	.262	.219
17	−.996	−.587	−.571	−.625
18	−1.869	−1.384	−1.321	−1.372
19	−2.270	−1.865	−1.772	−1.809
20	−1.294	−1.137	−1.071	−1.083
21	−1.147	−.901	−.834	−.824
22	−1.310	−1.040	−.954	−.924
23	−2.135	−1.734	−1.576	−1.496
24	−1.111	−.795	−.702	−.660
25	−.980	−.752	−.673	−.643
26	−.992	−.761	−.688	−.653
27	−1.020	−.764	−.689	−.653
28	−1.020	−.754	−.680	−.651
29	−1.000	−.758	−.678	−.653
30	−1.008	−.764	−.685	−.651

TABLE IV.—THEORETICAL PRESSURE DISTRIBUTION AROUND CYLINDER FOR WHICH $l=1$, $a=0$, AND $R=1.26$

$$\left[z=\zeta-\frac{1}{2}\frac{1}{\zeta^2}\right]$$

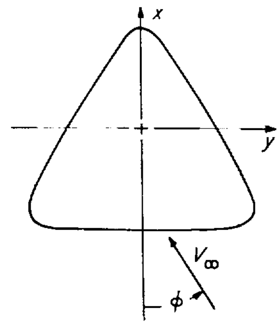

x/c_o	y/c_o	C_p for $\phi=$:				
		0	10	30	60	90
−0. 5	0. 0000	1. 0000	0. 9464	0. 5555	−0. 3336	−0. 7780
−. 49996	−. 1296	. 9430	. 7789	. 2189	−. 6695	−. 8337
−. 4991	−. 2514	. 7325	. 4284	−. 3416	−1. 2172	−1. 0187
−. 4955	−. 3583	. 1999	−. 3222	−1. 4002	−2. 2004	−1. 4002
−. 4863	−. 4445	−1. 2036	−2. 1294	−3. 7093	−4. 1724	−2. 1294
−. 4786	−. 4786	−2. 6832	−3. 9432	−5. 8729	−5. 8729	−2. 6832
−. 4681	−. 5061	−5. 1122	−6. 8119	−9. 1023	−8. 1979	−3. 3039
−. 4546	−. 5270	−8. 4473	−10. 5649	−12. 9732	−10. 5649	−3. 6321
−. 4375	−. 5413	−10. 9952	−13. 1227	−14. 9944	−10. 9952	−2. 9984
−. 4167	−. 5489	−10. 5649	−12. 1355	−12. 9725	−8. 4473	−1. 5146
−. 3918	−. 5502	−8. 1979	−9. 1020	−9. 1020	−5. 1127	−. 2188
−. 3627	−. 5455	−5. 8729	−6. 3104	−5. 8729	−2. 6832	. 5064
−. 3293	−. 5352	−4. 1732	−4. 3340	−3. 7099	−1. 2037	. 8392
−. 2500	−. 5000	−2. 2002	−2. 1037	−1. 4004	. 1999	1. 0000
−. 1556	−. 4497	−1. 2173	−1. 0187	−. 3416	. 7326	. 9311
−. 0498	−. 3895	−. 6695	−. 4180	. 2189	. 9500	. 7788
. 0625	−. 3248	−. 3335	−. 0433	. 5555	1. 0000	. 5555
. 1747	−. 2599	−. 1096	. 2187	. 7788	. 9430	. 2187
. 2797	−. 1983	. 0556	. 4286	. 9311	. 7326	−. 3412
. 3705	−. 1418	. 1999	. 6257	1. 0000	. 1999	−1. 4002
. 4406	−. 0906	. 3760	. 8392	. 8392	−1. 2034	−3. 7093
. 4662	−. 0669	. 5064	. 9440	. 5064	−2. 6832	−5. 8729
. 4849	−. 0441	. 6859	1. 0000	−. 2182	−5. 1127	−9. 1026
. 4962	−. 0219	. 8930	. 8937	−1. 5137	−8. 4447	−12. 9672
. 5	. 0000	1. 0000	. 5178	−2. 9984	−10. 9960	−14. 9936
. 4962	. 0219	. 8920	. 0574	−3. 6305	−10. 5608	−12. 9672
. 4849	. 0441	. 6859	−. 2182	−3. 3036	−8. 1979	−9. 1026
. 4662	. 0669	. 5064	−. 3157	−2. 6832	−5. 8729	−5. 8729
. 4406	. 0906	. 3760	−. 3222	−2. 1297	−4. 1722	−3. 7093
. 3705	. 1418	. 1999	−. 3333	−1. 4002	−2. 2004	−1. 4002
. 2797	. 1983	. 0556	−. 3412	−1. 0183	−1. 2167	−. 3412
. 1747	. 2599	−. 1096	−. 4178	−. 8334	−. 6693	. 2189
. 0625	. 3248	−. 3335	−. 5700	−. 7781	−. 3335	. 5555
−. 0498	. 3895	−. 6695	−. 8336	−. 8336	−. 1095	. 7788
−. 1556	. 4497	−1. 2173	−1. 2864	−1. 0189	. 0554	. 9311
−. 2500	. 5000	−2. 2002	−2. 1037	−1. 4004	. 1999	1. 0000
−. 3293	. 5352	−4. 1732	−3. 7099	−2. 1301	. 3762	. 8392
−. 3627	. 5455	−5. 8729	−5. 0504	−2. 6832	. 5164	. 5064
−. 3918	. 5502	−8. 1979	−6. 8125	−3. 3036	. 6859	−. 2188
−. 4167	. 5489	−10. 5649	−8. 4440	−3. 6305	. 8930	−1. 5137
−. 4375	. 5413	10. 9952	−8. 3850	−2. 9984	1. 0000	−2. 9984
−. 4546	. 5270	−8. 4473	−6. 0401	−1. 5146	. 8930	−3. 6321
−. 4681	. 5061	−5. 1122	−3. 3039	−. 2185	. 6859	−3. 3039
−. 4786	. 4786	−2. 6832	−1. 4235	. 5064	. 5064	−2. 6832
−. 4863	. 4445	−1. 2036	−. 3333	. 8392	. 3761	−2. 1294
−. 4955	. 3583	. 1999	. 6257	1. 0000	. 1999	−1. 4002
−. 4991	. 2514	. 7325	. 9357	. 9311	. 0554	−1. 0187
−. 49996	. 1296	. 9430	1. 0000	. 7789	−. 1095	−. 8337

TABLE V. THEORETICAL PRESSURE DISTRIBUTION AROUND CYLINDER FOR WHICH $l=1$, $a=0.2$, AND $R=1.533$

$$\left[z=\zeta-\frac{1}{2}\frac{1}{\zeta^2}\right]$$

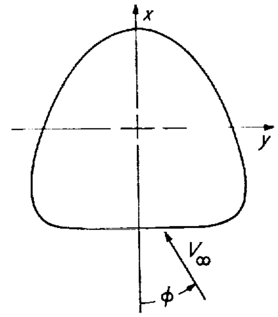

x/c_o	y/c_o	C_p for ϕ—:				
		0	10	30	60	90
−0.5000	0.0000	1.0000	0.9484	0.5056	−0.4823	−0.9776
−.4999	−.1272	.9354	.7493	.1144	−.8928	−1.0790
−.4990	−.2447	.6805	.3172	−.6027	−1.6486	−1.4116
−.4922	−.3445	−.0170	−.6808	−2.0512	−3.0685	−2.0512
−.4748	−.4222	−1.7508	−2.9066	−4.8788	−5.4568	−2.9066
−.4706	−.4521	−3.1169	−4.5253	−6.6821	−6.6821	−3.1169
−.4422	−.4764	−4.4532	−5.9697	−8.0132	−7.2063	−2.8399
−.4193	−.4951	−5.1957	−6.5844	−8.1638	−6.5844	−2.0378
−.3919	−.5086	5.1425	−6.2319	−7.1904	−5.1425	−1.0475
−.3599	−.5172	−4.6077	−5.3693	−5.7752	−3.5809	−.2193
−.3238	−.5215	−3.9502	−4.4368	−4.4368	−2.2898	.3441
−.2836	−.5216	−3.3139	−3.5886	−3.3139	−1.3118	.6902
−.2400	−.5180	−2.8490	−2.9686	−2.5043	−.6396	.8803
−.1444	−.5013	−2.1284	−2.0340	−1.3465	.2179	1.0000
−.0418	−.4733	−1.6551	−1.4174	−.6065	.6798	.9175
.0629	−.4358	−1.3132	−.9648	−.0823	.9210	.6935
.1645	−.3901	−1.0266	−.5856	.3245	1.0000	.3245
.2586	−.3371	−.7434	−.2276	.6525	.9104	−.2276
.3411	−.2778	−.4209	.1402	.8963	.5977	−1.0180
.4087	−.2132	−.0308	.5177	1.0000	−.0308	−2.0924
.4588	−.1446	.4178	.8500	.8500	−1.0559	−3.3941
.4867	−.1090	.6376	.9589	.6376	−1.7045	−4.0466
.4896	−.0730	.8257	1.0000	.3238	−2.3930	−4.6076
.4974	−.0366	.9541	.9589	−.0782	−3.0510	−4.9907
.5000	.0000	1.0000	.8152	−.5328	−3.5987	−5.1312
.4974	.0366	.9541	.5957	−.9861	−3.9586	−4.9907
.4896	.0730	.8257	.3238	−1.3888	−4.1055	−4.6076
.4867	.1090	.6376	.0340	−1.7045	−4.0466	−4.0466
.4588	.1446	.4178	−.2440	−1.9202	−3.8260	−3.3941
.4087	.2132	−.0308	−.7035	−2.0924	−3.1234	−2.0924
.3411	.2778	−.4209	−1.0180	−2.0367	−2.3353	−1.0180
.2586	.3371	−.7434	1.2283	−1.8814	1.6235	−.2276
.1645	.3901	−1.0266	−1.3861	1.7023	1.0266	.3245
.0629	.4358	−1.3132	−1.5406	1.5406	−.5373	.6935
−.0418	.4733	−1.6551	−1.7377	−1.4174	−.1311	.9175
−.1444	.5013	−2.1284	−2.0340	−1.3465	.2179	1.0000
−.2400	.5180	−2.8490	−2.5043	−1.3289	.2359	.8803
−.2836	.5216	−3.3139	−2.7977	−1.3118	.6902	.6902
−.3238	.5215	−3.9502	−3.2046	−1.3161	.8310	.3441
−.3599	.5172	−4.6077	−3.5809	−1.2461	.9481	−.2193
−.3919	.5086	−5.1425	−3.8058	1.0475	1.0000	−1.0475
−.4193	.4951	−5.1957	−3.6170	−.6491	.9298	−2.0379
−.4422	.4764	−4.4532	−2.8399	−.0871	.7198	−2.8399
−.4706	.4521	−3.1169	−1.7089	.4483	.4483	−3.1169
−.4748	.4222	−1.7508	−.6644	.7993	.2212	−2.9066
−.4922	.3445	−.0170	.5241	1.0000	−.0170	2.0512
−.4990	.2447	.6805	.9232	.9177	−.1284	−1.4116
−.4999	.1272	.9354	1.0000	.7493	−.2579	−1.0790

TABLE VI.—THEORETICAL PRESSURE DISTRIBUTION AROUND CYLINDER FOR WHICH $l=1$, $a=0.5$, AND $R=1.968$

$$\left[z=\zeta-\frac{1}{2}\frac{1}{\zeta^2}\right]$$

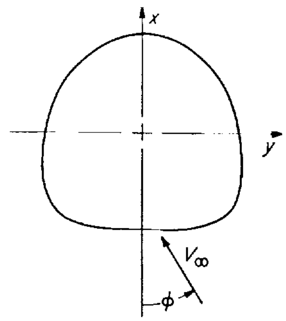

x/c_o	y/c_o	C_p for $\phi=$:				
		0	10	30	60	90
-0.5000	0.0000	1.0000	0.9304	0.4227	-0.7321	-1.3093
-.4994	-.1221	.9232	.7019	-.0529	-1.2504	-1.4717
-.4950	-.2242	.6157	.1788	-.9276	-2.1857	-1.9006
-.4807	-.3134	-.2149	1.0077	-2.6447	-3.8599	-2.6447
-.4510	-.3833	1.6254	-2.7285	-4.6108	-5.1625	-2.7285
-.4292	-.4115	-2.2776	-3.3988	-5.1160	-5.1160	-2.2776
-.4029	-.4355	-2.7008	-3.7300	-5.1168	-4.5692	-1.6059
-.3721	-.4557	-2.8870	-3.7582	-4.7491	-3.7582	-.9058
-.3372	-.4722	-2.9118	-3.6056	-4.2160	-2.9118	-.3039
-.2986	-.4855	-2.8545	-3.3779	-3.6569	-2.1487	.1619
-.2569	-.4955	-2.7646	-3.1347	-3.1347	-1.5019	.5012
-.2126	-.5025	-2.6703	-2.9040	2.6703	-.9670	.7364
-.1662	-.5062	-2.5778	-2.6890	-2.2574	-.5241	.8888
-.0696	-.5045	-2.3999	-2.2973	-1.5501	.1500	1.0000
.0286	-.4903	-2.2032	-1.9164	-.9382	.6137	.9004
.1246	-.4635	-1.9482	-1.5042	-.3795	.8993	.6093
.2149	-.4245	-1.6026	-1.0363	.1325	1.0000	.1325
.2965	-.3740	-1.1533	-.5162	.5707	.8894	-.5162
.3668	-.3130	-.6155	.0225	.8821	.5426	-1.2943
.4238	-.2430	-.0400	.5134	1.0000	-.0400	-2.1201
.4660	-.1657	.4874	.8679	.8679	-.8102	-2.8689
.4806	-.1256	.7006	.9660	.7006	-1.2346	-3.1698
.4913	-.0843	.8633	1.0000	.4696	-1.6613	-3.3984
.4978	-.0423	.9652	.9655	.1827	-2.0708	-3.5412
.5000	.0000	1.0000	.8616	-.1475	-2.4429	-3.5903
.4978	.0423	.9652	.6935	-.5055	-2.7588	-3.5412
.4913	.0843	.8633	.4696	-.8736	-3.0045	-3.3984
.4806	.1256	.7006	.2018	-1.2346	-3.1698	-3.1698
.4660	.1657	.4874	-.0954	-1.5712	-3.2493	-2.8689
.4238	.2430	-.0400	-.7187	-2.1201	-3.1603	-2.1201
.3668	.3130	-.6155	1.2943	-2.4526	-2.7921	-1.2943
.2965	.3740	-1.1533	-1.7523	-2.5590	-2.2404	-.5162
.2149	.4245	-1.6026	-2.0642	-2.4703	-1.6026	.1325
.1246	.4635	-1.9482	-2.2381	-2.2381	-.9593	.6093
.0286	.4903	-2.2032	-2.3028	1.9164	-.3645	.9004
-.0696	.5045	-2.3999	-2.2973	-1.5501	.1500	1.0000
-.1662	.5062	-2.5778	-2.2574	-1.1648	.5686	.8888
-.2126	.5025	-2.6703	-2.2311	-.9670	.7364	.7364
-.2569	.4955	-2.7646	-2.1976	-.7614	.8715	.5012
-.2986	.4855	-2.8545	-2.1487	-.5438	.9643	.1619
-.3372	.4722	-2.9118	-2.0606	-.3039	1.0000	-.3039
-.3721	.4557	-2.8870	-1.8965	-.0346	.9560	-.9058
-.4029	.4355	-2.7008	-1.6059	.2622	.8098	-1.6059
-.4292	.4115	-2.2776	-1.1566	.5608	.5608	-2.2776
-.4510	.3833	-1.6254	-.5885	.8084	.2567	-2.7285
-.4807	.3134	-.2149	.4315	1.0000	-.2149	-2.6447
-.4950	.2242	.6157	.9076	.9010	-.3571	-1.9006
-.4994	.1221	.9232	1.0000	.7019	-.4956	-1.4717

TABLE VII.—THEORETICAL PRESSURE DISTRIBUTION AROUND CYLINDER FOR WHICH $l=1$, $a=1$, AND $R=2.55$

$$\left[z=\zeta-\frac{1}{2}\frac{1}{\zeta^2}\right]$$

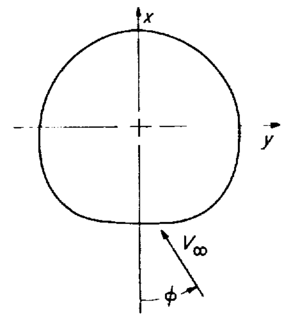

x/c_o	y/c_o	C_p for $\phi=$:				
		0	10	30	60	90
0.5000	0.0000	1.0000	0.9251	0.3785	-0.8645	-1.4859
-.4999	-.1119	.9140	.6662	-.1792	-1.5202	-1.7680
-.4946	-.2105	.5337	.0036	-1.3389	-2.8653	-2.5193
-.4747	-.2914	-.3280	-1.1946	-2.9840	-4.3123	-2.9840
-.4352	-.3569	-1.2698	-2.2235	-3.8509	-4.3279	-2.2235
-.4081	-.3850	-1.5990	-2.4882	-3.8499	-3.8499	-1.5990
-.3769	-.4103	-1.8411	-2.6312	-3.6959	-3.2755	-1.0006
-.3418	-.4329	-2.0283	-2.7070	-3.4790	-2.7070	-.4848
-.3035	-.4528	-2.1840	-2.7487	-3.2455	-2.1840	-.0613
-.2626	-.4699	-2.3174	-2.7679	-3.0080	-1.7100	.2787
-.2195	-.4840	-2.4351	-2.7728	-2.7728	-1.2829	.5448
-.1747	-.4950	-2.5330	-2.7580	-2.5331	-.8934	.7463
-.1288	-.5028	-2.6084	-2.7206	-2.2853	-.5372	.8888
-.0350	-.5079	-2.6721	-2.5613	-1.7542	.0820	1.0000
.0586	-.4988	-2.5784	-2.2580	-1.1652	.5685	.8888
.1491	-.4753	-2.3130	-1.8140	-.5501	.8869	.5610
.2337	-.4377	-1.8755	-1.2498	.0415	1.0000	.0415
.3100	-.3871	-1.3020	.6209	.5411	.8817	-.6209
.3757	-.3248	-.6558	-.0019	.8792	.5312	-1.3515
.4289	-.2527	-.0193	.5230	1.0000	-.0193	-2.0581
.4680	-.1729	.5159	.8753	.8753	-.7093	-2.6532
.4819	-.1308	.7214	.9684	.7214	-1.0792	-2.8798
.4920	-.0878	.8742	1.0000	.5120	-1.4489	-3.0473
.4980	-.0441	.9682	.9684	.2523	-1.8092	-3.1543
.5000	.0000	1.0000	.8738	.0463	-2.1392	-3.1854
.4980	.0441	.9682	.7196	-.3772	-2.4386	-3.1543
.4920	.0878	.8742	.5120	-.7241	-2.6849	-3.0473
.4819	.1308	.7214	.2573	-1.0792	-2.8798	-2.8798
.4680	.1729	.5159	-.0343	-1.4279	-3.0124	-2.6532
.4289	.2527	-.0193	-.6846	-2.0581	-3.0776	-2.0581
.3757	.3248	-.6558	-1.3515	-2.5387	-2.8866	-1.3515
.3100	.3871	-1.3020	-1.9423	-2.8047	-2.4641	-.6209
.2337	.4377	-1.8755	-2.3855	-2.8342	-1.8755	-.0415
.1491	.4753	-2.3130	-2.6387	-2.6387	-1.2018	-.5610
.0586	.4988	-2.5784	-2.6897	-2.2580	-.5244	-.8888
-.0350	.5079	-2.6721	-2.5613	-1.7542	.0820	1.0000
-.1288	.5028	-2.6084	-2.2853	-1.1833	.5649	.8888
-.1747	.4950	-2.5330	-2.1103	-.8934	.7463	.7463
-.2195	.4840	-2.4351	-1.9177	-.6073	.8827	.5448
-.2626	.4699	-2.3174	-1.7100	-.3287	.9693	.2787
-.3035	.4528	-2.1840	-1.4911	-.0638	1.0000	-.0613
-.3418	.4329	-2.0283	-1.2566	.1940	.9657	-.4848
-.3769	.4103	-1.8411	-1.0006	.4336	.8540	-1.0006
-.4081	.3850	-1.5990	-.7102	.6517	.6517	-1.5990
-.4352	.3569	-1.2698	-.3734	.8344	.3574	-2.2235
-.4747	.2914	-.3280	.3786	1.0000	-.3280	-2.9840
-.4946	.2105	.5337	.8879	.8798	-.6467	-2.5193
-.4999	.1119	.9140	1.0000	.6662	-.6748	-1.7680

TABLE VIII.- THEORETICAL PRESSURE DISTRIBUTION AROUND CYLINDER FOR WHICH $l=0.51764$, $a=0.5$, AND $R=2$

$$\left[z=\zeta-\frac{1-l^2}{\zeta}-\frac{1}{2}\frac{1}{\zeta^2}\right]$$

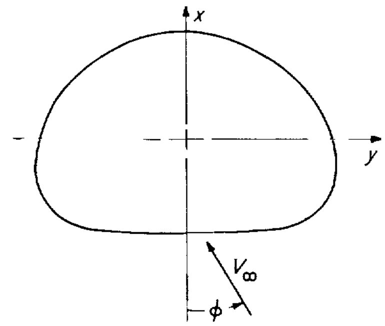

x/c_o	y/c_o	C_p for $\phi=$:				
		0	10	30	60	90
−0.5000	0.0000	1.0000	0.9449	0.5427	−0.3720	−0.8292
−.4997	−.1612	.9404	.7689	.1837	−.7445	−.9161
−.4968	−.3123	.7113	.3831	−.4480	−1.3929	−1.1788
.4860	−.4424	.1387	−.0265	−1.5840	−2.4455	−1.5840
−.4612	−.5485	−1.0625	−1.9291	−3.4078	−3.8411	−1.9291
−.4424	−.5923	1.9295	−2.9317	−4.4665	4.4665	−1.9295
−.4192	−.6301	−2.8776	−3.9559	−5.4089	−4.8351	−1.7304
−.3912	−.6620	−3.7462	4.8101	−6.0200	4.8101	−1.2371
−.3591	−.6883	4.3928	−5.3493	6.1907	−4.3928	−.7976
−.3235	−.7092	4.7491	−5.5298	−5.9459	−3.6964	−.2500
−.2838	−.7248	−4.8486	−5.4186	−5.4236	−2.8869	.2250
−.2416	−.7352	−4.7619	−5.1288	−4.7619	−2.0878	.5862
−.1874	−.7404	−4.5571	−4.7284	−4.0594	−1.3673	.8272
−.1003	−.7364	−3.9788	−3.8286	−2.7344	−.2447	1.0000
−.0011	−.7130	−3.3052	−2.9197	−1.6049	.4809	.8662
.0985	−.6713	−2.5953	−2.0537	−.6822	.8772	.5236
.1936	−.6121	−1.8678	−1.2438	.0441	1.0000	.0441
.2804	−.5369	−1.1468	−.5117	.5720	.8897	−.5117
.3557	−.4477	−.4667	.1125	.8930	.5848	−1.0830
.4174	−.3467	.1301	.5930	1.0000	.1301	−1.6098
.4641	−.2364	.5980	.8964	.8964	−.4194	−2.0336
.4791	−.1787	.7708	.9740	.7708	−.7103	−2.3089
.4906	−.1191	.8971	1.0000	.6010	−1.0021	−2.3803
.4982	−.0601	.9741	.9742	.3916	1.2858	−2.2803
.5000	.0000	1.0000	.8968	.1443	−1.5673	−2.4229
.4982	.0601	.9741	.7719	−.1207	−1.7979	−2.3803
.4906	.1191	.8971	.6010	−.4096	−2.0126	−2.3089
.4791	.1787	.7708	.3891	−.7103	−2.1914	−2.1914
.4641	.2364	.5980	.1411	−1.0161	−2.3318	−2.0336
.4174	.3467	.1301	−.4377	−1.6098	−2.4799	−1.6098
.3557	.4477	−.4667	−1.0830	−2.1345	−2.4428	−1.0830
.2804	.5369	−1.1468	−1.7438	−2.5482	−2.2306	−.5117
.1936	.6121	−1.8678	−2.3764	−2.8239	−1.8678	.0441
.0985	.6713	−2.5953	−2.9487	−2.9487	−1.2894	.5236
−.0011	.7130	−3.3052	−3.4389	−2.9197	−.8340	.8662
−.1003	.7364	−3.9788	−3.8286	−2.7344	.2447	1.0000
−.1874	.7404	−4.5571	−4.0594	−2.3623	.3299	.8272
−.2416	.7352	4.7619	−4.0724	−2.0878	.5862	.5862
−.2838	.7248	4.8486	−3.9677	−1.7365	.8003	.2250
−.3235	.7092	−4.7491	−3.6964	−1.3027	.9468	−.2500
−.3591	.6883	−4.3928	−3.2193	−.7976	1.0000	−.7976
−.3912	.6620	−3.7462	−2.4755	−.2633	.9462	−1.3271
−.4192	.6301	−2.8776	−1.7304	.2264	.8008	−1.7304
−.4424	.5923	−1.9295	−.9505	.6074	.7320	−1.9295
−.4612	.5485	−1.0625	.3278	.8435	.3979	−1.9291
−.4860	.4424	.1387	.4841	1.0000	.1379	−1.5840
−.4968	.3123	.7113	.8411	.2557	−.0194	−1.1788
−.4997	.1612	.9404	1.0000	.7690	−.1588	−.9161

TABLE IX.—THEORETICAL PRESSURE DISTRIBUTION AROUND CYLINDER OF MODIFIED RECTANGULAR CROSS SECTION WITH $b_o > c_o$

[Calculations by method of reference 4]

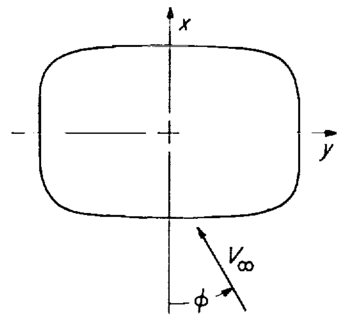

x/c_o	y/c_o	C_p for $\phi=$:				
		0	10	30	60	90
−0.5000	−0.0000	1.0000	0.9460	0.5527	−0.3417	−0.7889
−.5000	−.0870	.9853	.8709	.3659	−.5826	−.9124
−.4998	−.1724	.9385	.7613	.1569	−.8018	−.9791
−.4991	−.2545	.8496	.5987	−.1230	−1.0957	−1.0957
−.4973	−.3320	.6996	.3576	−.5081	−1.4921	−1.2690
−.4936	−.4037	.4555	−.0046	−1.0486	−2.0297	−1.5081
−.4871	−.4687	.0651	−.5503	−1.8140	−2.7515	−1.7158
−.4770	−.5264	−.5439	−1.3592	−2.8742	−3.6815	−2.1656
−.4621	−.5764	−1.4272	−2.4760	−4.2301	−4.7437	−2.4749
−.4419	−.6187	−2.5165	−3.7754	−5.6391	−5.6391	−2.5587
−.4157	−.6536	−3.4913	−4.8312	−6.5402	−5.8659	−2.2129
−.3830	−.6818	−3.9660	−5.1832	−6.4714	−5.1840	−1.4769
−.3437	−.7036	−3.8895	−4.8551	−5.6311	−3.9737	−.6574
−.2980	−.7201	−3.5222	−4.2169	−4.5491	−2.7521	.0014
−.2465	−.7322	−3.1081	−3.5772	−3.5775	−1.6700	.4480
−.1898	−.7406	−2.7626	−3.0533	−2.8114	−1.0430	.7263
−.1289	−.7460	−2.5157	−2.6539	−2.2401	−.5082	.8894
−.0652	−.7490	−2.3714	−2.4104	−1.8229	−.1305	.9739
.0000	−.7500	−2.3051	−2.2598	−1.5214	.1595	1.0000
.0652	−.7490	−2.3714	−2.2059	−1.3058	.3863	.9739
.1289	−.7460	−2.5157	−2.2397	−1.1533	.5708	.8894
.1898	−.7406	−2.7626	−2.3550	−1.0424	.7263	.7263
.2465	−.7322	−3.1081	−2.5396	−.9495	.8577	.4480
.2980	−.7201	−3.5222	−2.7511	−.8394	.9575	.0014
.3437	−.7036	−3.8895	−2.8905	−.6574	1.0000	−.6574
.3830	−.6818	−3.9660	−2.7641	−.3450	.9429	−1.4769
.4157	−.6536	−3.4913	−2.2120	.0907	.7658	−2.2129
.4419	−.6187	−2.5165	−1.3411	.5233	.5233	−2.5587
.4621	−.5764	−1.4272	−.4100	.8215	.3072	−2.4749
.4770	−.5264	−.5439	.1578	.9641	.1574	−2.1656
.4871	−.4687	.0651	.5612	1.0000	.0623	−1.7158
.4936	−.4037	.4555	.7954	.9768	−.0044	−1.5081
.4973	−.3320	.6996	.9225	.9225	−.0616	−1.2690
.4991	−.2545	.8496	.9829	.8496	−.1230	−1.0957
.4998	−.1724	.9385	1.0000	.7613	−.1975	−.9791
.5000	−.0870	.9853	.9854	.6675	−.2930	−.9124
.5000	−.0000	1.0000	.9460	.5527	−.3417	−.7889

TABLE X.—THEORETICAL PRESSURE DISTRIBUTION AROUND CYLINDER OF MODIFIED SQUARE CROSS SECTION ($b_o=c_o$)

[Calculations by method of reference 4]

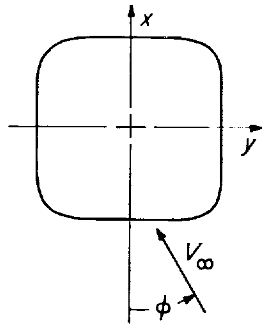

x/c_o	y/c_o	C_p for $\phi=$:			
		0	10	30	45
-0.5000	0.0000	1.0000	0.9322	0.4374	-0.1251
-.5000	-.0652	.9825	.8459	.2426	-.3512
-.4998	-.1289	.9256	.7115	-.0316	-.6552
-.4991	-.1898	.8145	.5055	-.3847	-1.0770
-.4973	-.2465	.6185	.1840	-.9133	-1.6784
-.4936	-.2980	.2824	-.3220	-1.6961	-2.5481
-.4871	-.3437	-.2856	-2.1722	-2.8570	-3.7979
-.4770	-.3830	-1.1912	-2.3301	-4.4711	-5.4589
-.4621	-.4157	-2.4098	-3.8428	-6.2871	-7.1894
-.4419	-.4419	-3.4994	-5.0378	-7.3968	-7.9972
-.4157	-.4621	-3.8425	-5.1892	-7.0033	-7.1894
-.3830	-.4770	-3.4694	-4.4711	-5.6094	-5.4584
-.3437	-.4871	-2.8570	-3.5412	-4.1423	-3.7979
-.2980	-.4936	-2.3030	-2.7384	-2.9876	-2.5481
-.2465	-.4973	-1.8790	-2.1661	-2.1622	-1.6784
-.1898	-.4991	-1.5834	-1.7480	-1.5834	-1.0770
-.1289	-.4998	-1.3921	-1.4666	-1.1778	-.6552
-.0652	-.5000	-1.2846	-1.2846	-.8909	-.3512
.0000	-.5000	-1.2500	-1.1821	-.6874	-.1251
.0652	-.5000	-1.2846	-1.1480	-.5446	.0488
.1289	-.4998	-1.3921	-1.1778	-.4474	.1886
.1898	-.4991	-1.5834	-1.2746	-.3847	.3078
.2465	-.4973	-1.8790	-1.4452	-.3472	.4177
.2980	-.4936	-2.3030	-1.6961	-.3220	.5301
.3437	-.4871	-2.8570	-2.0177	-.2857	.6555
.3830	-.4770	-3.4694	-2.3294	-.1897	.7990
.4157	-.4621	-3.8425	-2.4098	.0346	.9373
.4419	-.4419	-3.4994	-1.9616	.3974	1.0000
.4621	-.4157	-2.4098	-1.0633	.7513	.9373
.4770	-.3830	-1.1912	-.1911	.9494	.7990
.4871	-.3437	-.2856	.3985	1.0000	.6555
.4936	-.2980	.2824	.7307	.9695	.5301
.4973	-.2465	.6185	.9016	.9016	.4177
.4991	-.1898	.8145	.9790	.8145	.3078
.4998	-.1289	.9256	1.0000	.7115	.1886
.5000	-.0652	.9825	.9825	.5889	.0488
.5000	-.0000	1.0000	.9322	.4375	-.1251

TABLE XI.—THEORETICAL PRESSURE DISTRIBUTION AROUND CYLINDER OF MODIFIED RECTANGULAR CROSS SECTION WITH $b_o < c_o$

[Calculations by method of reference 4]

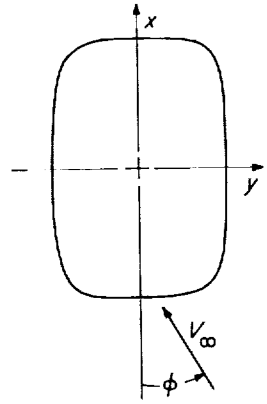

x/c_o	y/c_o	C_p for $\phi=$:				
		0	10	30	60	90
−0.5000	−0.0000	1.0000	0.8987	0.1595	1.5214	−2.3051
−.5000	.0435	.9739	.7698	−.1305	−1.8229	−2.3714
−.4998	.0860	.8894	.5706	−.5082	−2.2401	−2.5157
−.4991	−.1265	.7263	.2704	−1.0430	−2.8114	−2.7626
−.4973	−.1643	.4480	−.1794	−1.6700	−3.5775	−3.1081
.4936	−.1987	.0014	−.8397	−2.7521	−4.5491	−3.5222
−.4871	−.2291	−.6574	−1.7396	−3.9737	−5.6311	−3.8895
−.4770	−.2553	−1.4769	−2.7644	−5.7840	−6.4714	−3.9660
−.4621	−.2771	−2.2129	−3.5617	−5.8659	6.5402	−3.4913
−.4419	−.2946	−2.5587	−3.7758	−5.6391	−5.6391	−2.5165
−.4157	−.3081	−2.4749	−3.4419	−4.7437	−4.2301	−1.4272
−.3830	−.3180	−2.1656	−2.8828	−3.6815	−2.8742	−.5439
−.3437	−.3247	−1.7158	−2.3128	−2.7515	−1.8140	.0651
−.2980	−.3291	−1.5081	−1.8489	−2.0297	−1.0486	.4555
−.2465	−.3316	−1.2690	−1.5224	−1.4927	−.5081	.6996
−.1898	−.3327	−1.0957	−1.2259	−1.0957	−.1230	.8496
−.1289	−.3332	−.9791	−1.0406	−.8018	.1569	.9385
−.0652	−.3333	−.9124	−.9124	−.5826	.3659	.9853
.0000	−.3333	−.7889	−.7348	−.3417	.5527	1.0000
.0652	.3333	−.9124	−.7977	−.2930	.6675	.9853
.1289	−.3332	−.9791	−.8018	−.1975	.7613	.9385
.1898	−.3327	−1.0957	−.8448	−.1230	.8496	.8496
.2465	−.3316	−1.2690	−.9278	−.0616	.9225	.6996
.2980	−.3291	−1.5081	−1.0486	−.0044	.9768	.4555
.3437	−.3247	−1.7158	−1.2017	.0623	1.0000	.0651
.3830	−.3180	−2.1656	−1.3589	.1574	.9641	−.5439
.4157	−.3081	−2.4749	−1.4470	.3072	.8215	−1.4272
.4419	−.2946	−2.5587	−1.2400	.5233	.5233	−2.5165
.4621	−.2771	−2.2129	−.9439	.7658	.0907	−3.4913
.4770	−.2553	−1.4769	−.3443	.9429	−.3450	−3.9660
.4871	−.2291	.6574	.2250	1.0000	−.6574	−3.8895
.4936	−.1987	.0014	.6256	.9575	−.8394	−3.5222
.4973	−.1643	.4480	.8577	.8577	−.9495	−3.1081
.4991	−.1265	.7263	.9690	.7263	−1.0424	−2.7626
.4998	−.0860	.8894	1.0000	.5708	−1.1533	−2.5157
.5000	.0435	.9739	.9739	.3863	−1.3058	−2.3714
.5000	−.0000	1.0000	.8987	.1595	−1.5214	−2.3051

U.S. GOVERNMENT PRINTING OFFICE: 1960